

# Can Adversarial Examples Be Parsed to Reveal Victim Model Information?

Yuguang Yao<sup>1\*</sup>, Jiancheng Liu<sup>1\*</sup>, Yifan Gong<sup>2\*</sup>, Xiaoming Liu<sup>1</sup>, Yanzhi Wang<sup>2</sup>, Xue Lin<sup>2</sup>, Sijia Liu<sup>1,3</sup>  
<sup>1</sup>Michigan State University, <sup>2</sup>Northeastern University, <sup>3</sup>MIT-IBM Watson AI Lab

## Abstract

Numerous adversarial attack methods have been developed to generate imperceptible image perturbations that can cause erroneous predictions of state-of-the-art machine learning (ML) models, in particular, deep neural networks (DNNs). Despite extensive research on adversarial attacks (a.k.a., adversarial examples), little effort was made to uncover ‘arcana’ carried in these examples. In this study, we explore the feasibility of deducing data-agnostic information about the victim model (VM)—specifically, the characteristics of the ML model or DNN targeted for attack generation—from data-specific adversarial examples. We refer to this process as model parsing of adversarial attacks. We approach the model parsing problem as a supervised learning task, aiming to attribute categories of VM characteristics (including architecture type, kernel size, activation function, and weight sparsity) to individual adversarial examples. To this end, we have assembled a model parsing dataset featuring adversarial attacks spanning 7 distinct types, sourced from 135 victim models. These models are systematically varied across 5 architecture types, 3 kernel size configurations, 3 activation function categories, and 3 levels of weight sparsity ratios. We demonstrate that a simple, supervised model parsing network (MPN) is possible to uncover concealed details of the VM from adversarial examples. We also validate the practicality of model parsing from adversarial attacks by examining the effects of diverse training and evaluation factors on parsing performance. This includes investigating the impact of the formats of input attacks used for parsing and assessing generalization capabilities in out-of-distribution scenarios. Furthermore, we show how the proposed MPN can reveal the source VM attributes in transfer attacks, shedding light on a potential connection between model parsing and attack transferability. Code is available at <https://github.com/OPTML-Group/RED-adv>.

## 1. Introduction

Adversarial attacks, in terms of tiny (imperceptible) input perturbations crafted to *fool* the decisions of machine

\*Equal contributions.

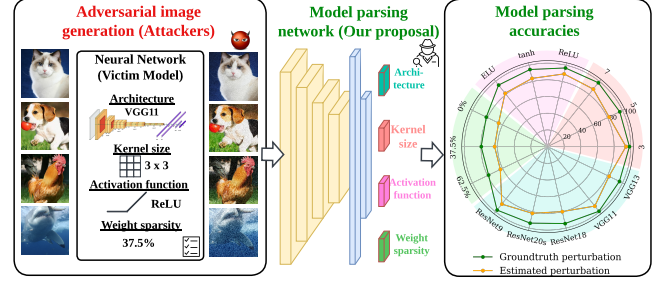


Figure 1. Schematic overview of model parsing from adversarial attacks. (Left) Attack generation leveraging the VM (victim model), with model attributes including architecture type, kernel size, activation function, and weight sparsity. (Middle) Proposed model parsing network (MPN), aiming to classify VM attributes based on adversarial examples. (Right) Demonstrating the efficacy of MPN in accurately parsing model attributes from PGD attacks [1] against ResNet9 on CIFAR-10. Performance metrics for MPN are showcased across two distinct types of input: actual adversarial perturbations and estimated adversarial perturbations, detailed in Sec. 4.

learning (ML) models, have emerged as a primary security concern of ML in a wide range of vision applications[2–11]. Therefore, a vast amount of prior works have been devoted to answering the questions of *how to generate* adversarial attacks for adversarial robustness evaluation [1, 3, 12–21] and *how to defend* against these attacks for robustness enhancement [1, 22–38]. These two questions are also closely interrelated, with insights from one contributing to the understanding of the other.

In the plane of attack generation, a variety of attack methods have been developed, ranging from gradient-based (white-box, perfect-knowledge) attacks [1, 3, 12, 13, 18, 20] to query-based (black-box, restricted-knowledge) attacks [14–17, 21]. Understanding the attack generation process allows us to further understand attacks’ characteristics and their specialties. For example, unlike Deepfake images that are created using generative models [39–45], adversarial examples are typically generated through a distinct process involving (a) a simple, deterministic perturbation optimizer (e.g., fast gradient sign method in [3]), (b) a specific input example (e.g., an image), and (c) a targeted, well-trained victim model (VM), i.e., an ML model that the adversary aims to compromise. In this context, both (a) and (b) interact with and depend on the VM for the generation of attacks.

The creation of adversarial examples also plays a pivotal role in advancing the development of adversarial defenses, such as robust training [1, 22–27, 37], adversarial detection [28–33, 46], and adversarial purification [34–36, 47].

Beyond traditional attack generation and defensive strategies, recent research [28, 48–55] has begun to explore and analyze adversarial attacks within a novel adversarial learning framework known as reverse engineering of deception (RED) [56]. It aims to infer the adversary’s information (e.g., the attack objective and adversarial perturbations) from attack instances. Yet, nearly all the existing RED approaches focused on either estimation/attribution of adversarial perturbations [49, 51–53] or recognition of attack classes/types [28, 48, 50, 54, 55]. None of the prior works investigated the feasibility of inferring *VM attributes* from adversarial examples, despite the foundational role of the VM in the attack generation. Thus, we ask (Q):

*(Q) Can adversarial examples be parsed to reveal VM information, such as architecture type, kernel size, and activation function?*

We refer to the problem encapsulated by question (Q) as **model parsing** of adversarial attacks. For a visual representation of this concept, please refer to **Fig. 1** for an illustrative overview. This work draws inspiration from the concept of model parsing as applied to generative models (GM) [40], a process aimed at inferring GM hyperparameters from synthesized photo-realistic images [40]. Unlike the scenario with GMs, where model attributes are embedded in the generated content, adversarial attacks represent data-specific perturbations formulated through meticulously designed optimizers, not GMs. The ‘model attributes’ subject to extraction from these adversarial instances pertain to the VM, which exhibits a less direct relationship with the perturbed data than the connection between GMs and their synthesized outputs [39, 40, 42–44]. Consequently, VM attributes have a subtler influence on the adversarial data, making the task of parsing these attributes inherently more challenging compared to decoding data-independent attributes of GMs. The proposed model parsing study also has an impact by enabling the inference of ‘attack toolchains’, in terms of the VM attributes embedded in adversarial attacks. This capability aligns with the objectives highlighted in the DARPA RED program, underscoring the strategic importance of understanding and mitigating adversarial tactics [56].

**A motivational scenario of model parsing through transfer attacks.** The potential of our model parsing approach can also be demonstrated in the scenario of transfer attacks. Consider a situation where adversarial examples are crafted using model A but are employed to compromise model B in a transfer attack setting (refer to **Fig. 2** for a visual guide).

Through effective model parsing, it becomes feasible to trace back and identify the original model A that served as the source for these adversarial samples, thereby revealing the concealed VM information of the transfer attack. It’s also worth highlight that our investigation is driven by the perspective of a reverse engineer rather than an adversary. Our objective is to deconstruct and understand the origin and characteristics of adversarial examples found in the wild, not to leverage adversarial techniques to extract information from a targeted, opaque model. This distinction underscores our commitment to enhancing security measures rather than undermining them.

**Contributions.** We summarize our contributions below.

- To the best of our knowledge, we for the first time propose and formalize the concept of model parsing to unveil the VM attributes from adversarial attacks.
- We approach the model parsing problem of adversarial attacks as a supervised learning task and show that the model parsing network (MPN) could exhibit a surprising amount of generalization to recognize VM attributes from testing attack instances (Fig. 1). We also peer into the influence of designing factors (including input data format, backbone network, and evaluation metric) in MPN’s generalization.
- We make a comprehensive study on the feasibility and effectiveness of model parsing from adversarial attacks, including in-distribution generalization as well as out-of-distribution generalization on unseen attack types and model architectures. We also demonstrate how the model parsing approach can be used to uncover the true, source victim model attributes from transfer attacks (Fig. 2), and show a connection between model parsing and attack transferability.

## 2. Related Work

**Adversarial attacks and defenses.** Intensive research efforts have been made for the design of adversarial attacks and defenses. Adversarial attacks in the digital domain [1, 3, 12–15, 17, 19, 21, 57–60] typically deceive DNNs by integrating carefully-crafted tiny perturbations into input data. Adversarial attacks in the physical domain [61–66] are further developed to fool victim models under complex physical environmental conditions, which require stronger adversarial

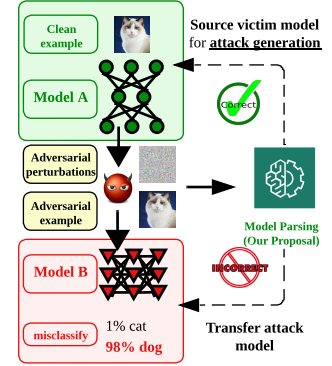


Figure 2. Model parsing in the context of transfer attacks: An effective model parsing system could accurately identify the original VM from which the adversarial attack was generated, as opposed to merely recognizing the target model intended for the transfer attack.

perturbations than digital attacks. In this work, we focus on the commonly-used digital attacks subject to  $\ell_p$ -norm based perturbation constraints, known as  $\ell_p$  attacks. Based on how an adversary interacts with the VM (victim model),  $\ell_p$  attacks also include both perfect-knowledge attacks (with full access to the VM based on which attacks are generated) and restricted-knowledge attacks (with access only to the VM’s input and output). The former typically leverages the local gradient information of VM to generate attacks [1, 3, 12], while the latter takes input-output queries of VM for attack generation [14, 15, 17, 21, 59, 60].

Given the vulnerability of ML models to adversarial attacks, methods to defend against these attacks are another research focus [1, 22–37, 46, 47, 67, 68]. One line of research is to advance model training methods to acquire adversarially robust models [1, 22–27, 37, 68]. Examples include min-max optimization-based adversarial training and its many variants [1, 22, 25–27, 37]. To make models provably robust, certified training is also developed by integrating robustness certificate regularization into model training [23, 69, 70] or leveraging randomized smoothing [24, 71, 72]. In addition to training robust models, another line of research on adversarial defense is to detect adversarial attacks by exploring and exploiting the differences between adversarial data and benign data [28–33, 46, 67].

**Reverse engineering of deception (RED).** RED has emerged as a new adversarial learning to extract insights into an adversary’s strategy, including their identity, objectives, and the specifics of their attack perturbations. For example, a few recent works [28, 48, 50, 54, 55] aim to reverse engineer the mechanisms behind attack generation, including the identification of the methods used and the specific hyperparameters (like perturbation radius and step count). In addition, other research efforts, exemplified by works [49, 51–53], have concentrated on estimating or pinpointing the specific adversarial perturbations employed in crafting adversarial imagery. This line of research is also related to the area of adversarial purification [34–36, 47], which aims to mitigate adversarial effects by identifying and eliminating their detrimental impact on model accuracy.

However, none of the prior works investigated the question of whether attributes of the VM can be reverse-engineered from adversarial attacks. The potential to parse VM attributes from adversarial attacks, if realized, could profoundly enhance our comprehension of the underlying threat models. Our study draws inspiration from the model parsing concept in GMs (generative models) [40], which focuses on inferring GM attributes from their synthesized images. This is based on the premise that GMs embed distinct fingerprints in their outputs, facilitating applications such as DeepFake detection and model attribute inference [39, 40, 42–44]. Lastly, we stress that RED diverges from efforts focused on reverse engineering black-box model hy-

perparameters [73, 74], which infer model attributes from a model’s prediction logits. Within our model parsing framework, information about the VM is not directly accessible from the adversarial attacks. Our methodology operates without any direct access to the VM, relying solely on adversarial examples gathered from attack generators.

### 3. Preliminaries and Problem Setups

**Preliminaries: Adversarial attack generation.** We first introduce different kinds of adversarial attacks and exhibit their dependence on **VM (victim model)**, *i.e.*, the ML model from which attacks are generated. Throughout the paper, we will focus on  $\ell_p$  attacks with  $p \in \{2, \infty\}$ , where the adversary aims to generate imperceptible input perturbations to fool an image classifier [3]. Let  $\mathbf{x}$  and  $\theta$  denote a benign image and the parameters of VM. The **adversarial attack** (*a.k.a.*, adversarial example) is defined via the linear perturbation model  $\mathbf{x}' = \mathbf{x} + \delta$ , where  $\delta = \mathcal{A}(\mathbf{x}, \theta, \epsilon)$  denotes **adversarial perturbations**, and  $\mathcal{A}$  refers to an attack generation method relying on  $\mathbf{x}$ ,  $\theta$ , and the attack strength  $\epsilon$  (*i.e.*, the perturbation radius of  $\ell_p$  attacks).

We focus on 7 attack methods given their different dependencies on the victim model ( $\theta$ ), including input gradient-based perfect-knowledge attacks with full access to  $\theta$  (FGSM [3], PGD [1], CW [12], and AutoAttack or AA [13]) as well as query-based restricted-knowledge attacks (ZO-signSGD [15], NES [16], and SquareAttack or Square [17]). Among the plethora of  $\ell_p$  attack techniques, the methods we have chosen to focus on are characterized by their diverse optimization strategies, loss functions,  $\ell_p$  norms, and dependencies on the VM’s parameters ( $\theta$ ). An overview of these selected methods is presented in **Table 1**.

Table 1. Summary of focused attack types. Here GD refers to gradient descent, and PK and RK refer to the perfect-knowledge and restricted-knowledge of the VM, respectively.

| Attacks                   | Generation method | Loss        | $\ell_p$ norm             | Strength $\epsilon$                           | Dependence on $\theta$                  |
|---------------------------|-------------------|-------------|---------------------------|---|---|
| FGSM                      | one-step GD       | CE          | $\ell_\infty$             | {4, 8, 12, 16}/255                            | PK, gradient-based                      |
| PGD                       | multi-step GD     | CE          | $\ell_\infty$<br>$\ell_2$ | {4, 8, 12, 16}/255<br>0.25, 0.5, 0.75, 1      | PK, gradient-based                      |
| CW                        | multi-step GD     | CW          | $\ell_2$                  | soft regularization<br>$c \in \{0.1, 1, 10\}$ | PK, gradient-based                      |
| AutoAttack<br>or AA       | attack ensemble   | CE /<br>DLR | $\ell_\infty$<br>$\ell_2$ | {4, 8, 12, 16}/255<br>0.25, 0.5, 0.75, 1      | PK, gradient-based +<br>RK, query-based |
| SquareAttack<br>or Square | random search     | CE          | $\ell_\infty$<br>$\ell_2$ | {4, 8, 12, 16}/255<br>0.25, 0.5, 0.75, 1      | RK, query-based                         |
| NES                       | ZOO               | CE          | $\ell_\infty$             | {4, 8, 12, 16}/255                            | RK, query-based                         |
| ZO-signSGD                | ZOO               | CE          | $\ell_\infty$             | {4, 8, 12, 16}/255                            | RK, query-based                         |

◆ FGSM (fast gradient sign method) [3]: This attack method is given by  $\delta = \mathbf{x} - \epsilon \times \text{sign}(\nabla_{\mathbf{x}} \ell_{\text{atk}}(\mathbf{x}; \theta))$ , where  $\text{sign}(\cdot)$  is the entry-wise sign operation, and  $\nabla_{\mathbf{x}} \ell_{\text{atk}}$  is the input gradient of a cross-entropy (CE)-based attack loss  $\ell_{\text{atk}}(\mathbf{x}; \theta)$

◆ PGD (projected gradient descent) [1]: This extends FGSM via an iterative algorithm. The  $K$ -step PGD  $\ell_\infty$  attack is given by  $\delta = \delta_K$ , where  $\delta_k = \mathcal{P}_{\|\delta\|_\infty \leq \epsilon}(\delta_{k-1} - \alpha \times \text{sign}(\nabla_{\mathbf{x}} \ell_{\text{atk}}(\mathbf{x}; \theta)))$  for  $k = 1, \dots, K$ ,  $\mathcal{P}_{\|\delta\|_\infty \leq \epsilon}$  is the projection operation onto the  $\ell_\infty$ -norm constraint  $\|\delta\|_\infty \leq \epsilon$ ,

and  $\alpha$  is the attack step size. By replacing the  $\ell_\infty$  norm with the  $\ell_2$  norm, we similarly obtain the *PGD  $\ell_2$  attack* [1].

◆ **CW (Carlini-Wager) attack** [12]: Similar to PGD, CW calls iterative optimization for attack generation. Yet, CW formulates attack generation as an  $\ell_p$ -norm regularized optimization problem, with the regularization parameter  $c = 1$  and  $p = 2$  by default. Here setting the regularization parameter  $c = 1$  can result in variations in the perturbation strengths ( $\epsilon$ ) across different CIFAR-10 images. However, the average perturbation strength tends to stabilize around  $\epsilon = 0.33$ . Moreover, CW adopts a hinge loss to ensure the misclassification margin.

◆ **AutoAttack (or AA)** [13]: This is an ensemble attack that uses AutoPGD, an adaptive version of PGD, as the primary means of attack. The loss of AutoPGD is given by the difference of logits ratio (DLR) rather than CE or CW loss.

◆ **ZO-signSGD** [15] and **NES** [16]: They are zeroth-order optimization (ZOO)-based restricted-knowledge attacks. In contrast to perfect-knowledge gradient-based attacks that have full access to the VM’s parameters ( $\theta$ ), restricted-knowledge attacks interact with the victim model solely through submitting inputs and receiving the corresponding predictions, without direct access to the model’s internal structure or gradients. ZOO then uses these input-output queries to estimate input gradients and generate adversarial perturbations. Yet, ZO-signSGD and NES call different gradient estimators in ZOO [75].

◆ **SquareAttack (or Square)** [17]: This attack is built upon random search and thus does not rely on the input gradient of the VM.

It is worth noting that we concentrate on  $\ell_\infty$  and  $\ell_2$  attacks as our exploration into the potential for model parsing from adversarial examples. *Our aim is not to exhaustively catalog all attack methods but to demonstrate a possibly novel avenue for reverse engineering of VM information carried by adversarial instances.*

**Model parsing of adversarial attacks.** It is clear that adversarial attacks contain the information of VM ( $\theta$ ), although the degree of their dependence varies. Thus, one may wonder if the *attributes* of  $\theta$  can be *inferred* from these attack instances, *i.e.*, adversarial perturbations/examples. The model attributes of our interest include model architectures as well as finer-level knowledge, *e.g.*, activation function type. We call the resulting problem **model parsing of adversarial attacks**, as described below.

**(Problem statement)** Is it possible to infer VM information from adversarial attacks? And what factors will influence such model parsing ability?

To the best of our knowledge, the feasibility of model parsing for adversarial attacks is an open question. Its challenges stay in two dimensions. **First**, through the **model lens**, VM is indirectly coupled with adversarial attacks, *e.g.*,

via local gradient information or model queries. Thus, it remains elusive what VM information is fingerprinted in adversarial attacks and impacts the feasibility of model parsing. **Second**, through the **attack lens**, the diversity of adversarial attacks (Table 1) makes a once-for-all model parsing solution extremely difficult. We thus take the first step to investigate the feasibility of model parsing and study what factors may influence its performance.

**Model attributes and setup.** We specify VMs as convolutional neural network (CNN)-based image classifiers used by attack generators. We consider 5 CNN architecture types (ATs): ResNet9, ResNet18, ResNet20, VGG11, and VGG13. Given an AT, CNN models are then configured by different choices of kernel size (KS), activation function (AF), and weight sparsity (WS). Thus, a valued quadruple (AT, KS, AF, WS) yields a specific VM ( $\theta$ ).

Although more attributes could be considered, we focus on KS and AF since they are the two fundamental building components of CNNs.

Table 2. Summary of model attributes of interest. Each attribute value corresponds to an attribute class in model parsing.

| Model attributes    | Code | Classes per attribute                       |
|---------------------|------|---|
| Architecture type   | AT   | ResNet9, ResNet18<br>ResNet20, VGG11, VGG13 |
| Kernel size         | KS   | 3, 5, 7                                     |
| Activation function | AF   | ReLU, tanh, ELU                             |
| Weight sparsity     | WS   | 0%, 37.5%, 62.5%                            |

Besides, we choose WS as another model attribute since it relates to sparse models achieved by pruning (*i.e.*, removing redundant model weights) [76, 77].

**Table 2** summarizes the model attributes and their values when specifying VM instances. Given a VM specification, adversarial attacks are generated following Table 1.

## 4. Methods

In this section, we approach the model parsing problem as a supervised learning task applied over the dataset of adversarial attacks. We will show that the learned model could exhibit a surprising amount of generalization on test-time adversarial data. We will also show data-model factors that may influence such generalization.

**Model parsing network and training.** We propose a parametric model, termed model parsing network (MPN), which takes adversarial attacks as input and predicts the model attribute values (*i.e.*, ‘classes’ in Table 2). It is worth noting that the proposed MPN operates solely on adversarial examples, possessing no prior information about the victim model, highlighting its capacity to unveil the secrets of VM embedded in adversarial examples. Despite the simplicity of supervised learning, the construction of MPN is non-trivial considering the factors such as the input data format, the choice of an appropriate backbone network, and the determination of suitable evaluation metrics.

First, we create a dataset by collecting adversarial examples against VMs. Since adversarial attacks are proposed

for evading model predictions after training, we choose the test set of an ordinary image dataset (e.g., CIFAR-10) to generate adversarial data, where an 80/20 training/test split is used for MPN training and evaluation. Following notations in Sec. 3, the training set of MPN is denoted by  $\mathcal{D}_{\text{tr}} = \{(\mathbf{z}(\mathcal{A}, \mathbf{x}, \boldsymbol{\theta}), y(\boldsymbol{\theta})) \mid \mathbf{x} \in \mathcal{I}_{\text{tr}}, \boldsymbol{\theta} \in \Theta\}$ , where  $\mathbf{z}$  denotes attack instances (e.g., adversarial perturbations  $\delta$  or adversarial example  $\mathbf{x}'$ ) that relies on the attack method  $\mathcal{A}$ , the original image sample  $\mathbf{x}$ , and the VM  $\boldsymbol{\theta}$ , and  $y(\boldsymbol{\theta})$  denotes the true model attribute label of  $\boldsymbol{\theta}$  associated with  $\mathbf{z}$ . To differentiate with the testing data of MPN, we denote by  $\mathcal{I}_{\text{tr}}$  the set of original images used for training MPN. We also denote by  $\Theta$  the set of VMs used for generating adversarial examples. For simplicity, we denote the training set of MPN as  $\mathcal{D}_{\text{tr}} = \{(\mathbf{z}, y)\}$  to omit the dependence on other factors.

Next, we study the construction of MPN (parameterized by  $\phi$ ). First, we manage to examine the *feasibility* of model parsing even forcing the *simplicity* of attribution network. Second, we manage to avoid the *model attribute bias* of  $\phi$  when inferring VM attributes. Therefore, we specify MPN by two simple networks: (1) multilayer perceptron (MLP) containing 2 hidden layers with 128 hidden units (0.41M parameters) [78], and (2) a simple 4-layer CNN (ConvNet-4) with 64 output channels for each layer, followed by one fully-connected layers with 128 hidden units and the attribution prediction head (0.15M parameters) [79]. We found that the model parsing accuracy using ConvNet-4 typically outperforms that of MLP. Thus, ConvNet-4 is designated as the default architecture for our MPN.

Given the datamodel setup, we next tackle the recognition problem of VM's attributes (AT, KS, AF, WS) via a multi-head multi-class classifier. We dissect MPN into two parts  $\phi = [\phi_{\text{rep}}, \phi_{\text{atr}}]$ , where  $\phi_{\text{rep}}$  is for data representation acquisition, and  $\phi_{\text{atr}}$  corresponds to the attribute-specific prediction head (i.e., the last fully-connected layer in our design). Eventually, four prediction heads  $\{\phi_{\text{atr}}^{(i)}\}_{i=1}^4$  will share  $\phi_{\text{rep}}$  for model attribute recognition; see Fig. 3 for a schematic overview of our proposal. The MPN training problem is then cast as

$$\underset{\phi_{\text{rep}}, \{\phi_{\text{atr}}^{(i)}\}_{i=1}^4}{\text{minimize}} \quad \mathbb{E}_{(\mathbf{z}, y) \in \mathcal{D}_{\text{tr}}} \sum_{i=1}^4 [\ell_{\text{CE}}(h(\mathbf{z}; \phi_{\text{rep}}, \phi_{\text{atr}}^{(i)}), y_i)], \quad (1)$$

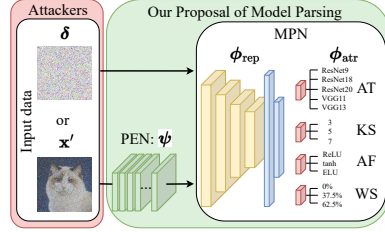


Figure 3. Model parsing via supervised learning. Adversarial examples or perturbations, crafted by attackers, serve as the input of MPN, which aims to decode VM attributes from adversarial inputs. The PEN (perturbation estimation network), introduced subsequently, acts as a preprocessing step, converting adversarial examples into inputs resembling perturbations.

where  $h(\mathbf{z}; \phi_{\text{rep}}, \phi_{\text{atr}}^{(i)})$  denotes the MPN prediction at input example  $\mathbf{z}$  using the predictive model consisting of  $\phi_{\text{rep}}$  and  $\phi_{\text{atr}}^{(i)}$  for the  $i$ th attribute classification,  $y_i$  is the ground-truth label of the  $i$ th attribute associated with the input data  $\mathbf{z}$ , and  $\ell_{\text{CE}}$  is the cross-entropy (CE) loss characterizing the error between the prediction and the true label.

**Evaluation methods.** Similar to training, we denote by  $\mathcal{D}_{\text{test}} = \{(\mathbf{z}(\mathcal{A}, \mathbf{x}, \boldsymbol{\theta}), y(\boldsymbol{\theta})) \mid \mathbf{x} \in \mathcal{I}_{\text{test}}, \boldsymbol{\theta} \in \Theta\}$  the test attack set for evaluating the performance of MPN. Here the set of benign images  $\mathcal{I}_{\text{test}}$  is different from  $\mathcal{I}_{\text{tr}}$ , thus adversarial attacks in  $\mathcal{D}_{\text{test}}$  are new to  $\mathcal{D}_{\text{tr}}$ . To mimic the standard evaluation pipeline of supervised learning, we propose the following evaluation metrics.

(1) *In-distribution generalization:* The MPN testing dataset  $\mathcal{D}_{\text{test}}$  follows the attack methods ( $\mathcal{A}$ ) and the VM specifications ( $\Theta$ ) same as  $\mathcal{D}_{\text{tr}}$  but corresponding to different benign images (i.e.,  $\mathcal{I}_{\text{test}} \neq \mathcal{I}_{\text{tr}}$ ). The purpose of such an in-distribution evaluation is to examine if the trained MPN can infer model attributes encoded in new attack data given existing attack methods.

(2) *Out-of-distribution (OOD) generalization:* In addition to new test-time images, there exist *attack/model distribution shifts* in  $\mathcal{D}_{\text{test}}$  due to using *new* attack methods or model architectures, leading to *unseen* attack methods ( $\mathcal{A}$ ) and victim models ( $\Theta$ ) different from the settings in  $\mathcal{D}_{\text{tr}}$ .

Unless specified otherwise, the generalization of MPN stands for the *in-distribution generalization*. Yet, both in-distribution and OOD generalization capabilities will be empirically assessed.

**Perturbations or adversarial examples? The input data format matters for MPN.** Recall from Sec. 3 that an adversarial example, given by the linear model  $\mathbf{x}' = \mathbf{x} + \delta$ , relates to  $\boldsymbol{\theta}$  through  $\delta$ . Thus, it could be better for MPN to adopt *adversarial perturbations* ( $\delta$ ) as the attack data feature ( $\mathbf{z}$ ), rather than the indirect adversarial example  $\mathbf{x}'$ . **Fig. 4** empirically justifies

our hypothesis by comparing the generalization of MPN trained on adversarial perturbations with that on adversarial examples under two model specifications of MPN, MLP and ConvNet-4. We present the performance of MPN trained and tested on different attack types. As we can see, the use

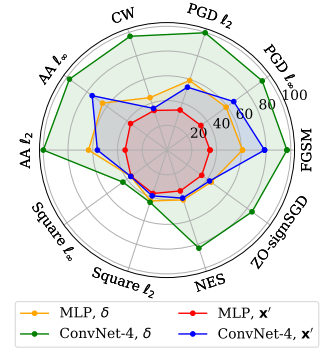


Figure 4. The VM attribute classification accuracy of MPN under different input formats (adversarial perturbations  $\delta$  vs. examples  $\mathbf{x}'$ ) and parsing networks (ConvNet-4 vs. MLP). The accuracy is measured in the context of in-distribution generalization. The attack data is generated from attack methods given in Table 1, with  $\ell_{\infty}$  attack strength  $\epsilon = 8/255$  and  $\ell_2$  attack strength  $\epsilon = 0.5$  on CIFAR-10.

of adversarial perturbations ( $\delta$ ) consistently improves the classification accuracy of VM attributes, compared to the use of adversarial examples ( $\mathbf{x}'$ ). In addition, ConvNet-4 outperforms MLP with a substantial margin.

Although Fig. 4 shows the promise of the generalization ability of MPN when trained and tested on adversarial perturbations, it may raise another practical question of how to obtain adversarial perturbations from adversarial examples if the latter is the only attack source accessible to MPN. To overcome this difficulty, we propose a *perturbation estimator network* (PEN) that can be jointly learned with MPN. Once PEN is prepended to the MPN model, the resulting end-to-end pipeline can achieve model parsing using adversarial examples as inputs (see the lower pipeline in Fig. 3). We use a denoising network, DnCNN [80], to model PEN with parameters  $\psi$ . PEN obtains perturbation estimates by minimizing the denoising objective using the true adversarial perturbations as supervision. Extended from (1), we have

$$\begin{aligned} & \text{minimize} \quad \beta \mathbb{E}_{(\mathbf{x}, \mathbf{x}') \in \mathcal{D}_{\text{tr}}} [\ell_{\text{MAE}}(g_{\psi}(\mathbf{x}'), \mathbf{x}' - \mathbf{x})] \\ & \psi, \phi_{\text{rep}}, \{\phi_{\text{att}}^{(i)}\}_{i=1}^4 \quad (2) \\ & + \mathbb{E}_{(\mathbf{x}', y) \in \mathcal{D}_{\text{tr}}} \sum_{i=1}^4 [\ell_{\text{CE}}(h(g_{\psi}(\mathbf{x}'); \phi_{\text{rep}}, \phi_{\text{att}}^{(i)}), y_i)], \end{aligned}$$

where  $g_{\psi}(\mathbf{x}')$  is output of PEN given  $\mathbf{x}'$  as input,  $\ell_{\text{MAE}}$  is the mean-absolute-error (MAE) loss characterizing the perturbation estimation error, and  $\beta > 0$  is a regularization parameter. Compared with (1), MPN is integrated with the perturbation estimation  $g_{\psi}(\mathbf{x}')$  for VM attribute classification.

## 5. Experiments

### 5.1. Experiment setup and implementation

**Dataset curation.** We use standard image classification datasets (CIFAR-10, CIFAR-100, and Tiny-ImageNet) to train VMs, from which attacks are generated. We refer readers to Appendix A for details on VM training and evaluation, as well as different attack setups. These VM instances are then leveraged to create the training and evaluation datasets of MPN, as described in Sec. 4. The attack types and victim model configurations have been summarized in Table 1 and 2. Eventually, we collect a dataset consisting of adversarial attacks across 7 attack types generated from 135 VMs (configured by 5 architecture types, 3 kernel size setups, 3 activation function types, and 3 weight sparsity levels).

**MPN training and evaluation.** To solve problem (1), we train the MPN model using the SGD (stochastic gradient descent) optimizer with cosine annealing learning rate schedule and an initial learning rate of 0.1. The training epoch number and the batch sizes are given by 100 and 256, respectively. To solve problem (2), we first train MPN according to (1), and then fine-tune a pre-trained DnCNN model [49] (taking only the denoising objective into consideration) for 20 epochs. Starting from these initial models, we jointly optimize MPN and PEN by minimizing problem (2) with

Table 3. The in-distribution testing accuracy (%) of MPN trained using different input data formats (adversarial examples  $\mathbf{x}'$ , PEN-estimated adversarial perturbations  $\delta_{\text{PEN}}$ , and true adversarial perturbations  $\delta$ ) across different attack types on CIFAR-10, with  $\ell_{\infty}$  attack strength  $\epsilon = 8/255$ ,  $\ell_2$  attack strength  $\epsilon = 0.5$ , and CW attack strength  $c = 1$ .

| Input data            | Attack type | FGSM  | PGD $\ell_{\infty}$ | PGD $\ell_2$ | CW    | AA $\ell_{\infty}$ | AA $\ell_2$ | Square $\ell_{\infty}$ | Square $\ell_2$ | NES   | ZO-signSGD |
|-----------------------|-------------|-------|---------------------|--------------|-------|--------------------|-------------|------------------------|-----------------|-------|------------|
| $\mathbf{x}'$         |             | 78.80 | 66.62               | 53.42        | 35.42 | 74.78              | 56.26       | 38.92                  | 36.21           | 40.80 | 42.48      |
| $\delta_{\text{PEN}}$ |             | 94.15 | 83.20               | 82.58        | 64.46 | 91.09              | 86.89       | 44.14                  | 42.30           | 58.85 | 61.20      |
| $\delta$              |             | 96.89 | 95.07               | 99.64        | 96.66 | 97.48              | 99.95       | 44.37                  | 44.05           | 83.33 | 84.87      |

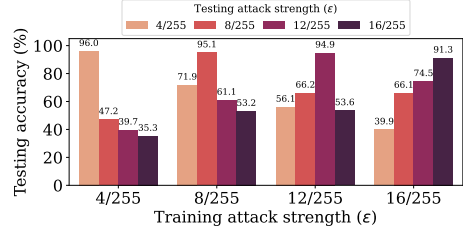


Figure 5. Testing accuracies (%) of MPN when trained on adversarial perturbations generated by PGD  $\ell_{\infty}$  using different attack strengths ( $\epsilon$ ) and evaluated using different attack strengths as well. Other setups are consistent with in Table 3.

$\beta = 1$  over 50 epochs. To evaluate the effectiveness of MPN, we consider both in-distribution and OOD generalization assessment. The generalization performance is measured by testing accuracy averaged over attribute-wise predictions, namely,  $\sum_i (N_i \text{TA}(i)) / \sum_i N_i$ , where  $N_i$  is the number of classes of the model attribute  $i$ , and  $\text{TA}(i)$  is the testing accuracy of the classifier associated with the attribute  $i$ .

### 5.2. Results and insights

**In-distribution generalization of MPN is achievable.** Table 3 presents the in-distribution generalization performance of MPN trained using different input data formats (i.e., adversarial examples  $\mathbf{x}'$ , PEN-estimated adversarial perturbations  $\delta_{\text{PEN}}$ , and true adversarial perturbations  $\delta$ ) given each attack type in Table 1. Here the choice of AT (architecture type) is fixed to ResNet9, but adversarial attacks on CIFAR-10 are generated from VMs configured by different values of KS, AF, and WS (see Table 2). As we can see, the generalization of MPN varies against the attack type even if model parsing is conducted from the ideal adversarial perturbations ( $\delta$ ). We also note that model parsing from perfect-knowledge adversarial attacks (i.e., FGSM, PGD, and AA) is easier than that from restricted-knowledge attacks (i.e., ZO-signSGD, NES, and Square). For example, the worst-case performance of MPN is achieved when training/testing on Square attacks. This is not surprising, since Square is based on random search and has the least dependence on VM attributes. In addition, we find that MPN using estimated perturbations ( $\delta_{\text{PEN}}$ ) substantially outperforms the one trained on adversarial examples ( $\mathbf{x}'$ ). This justifies the effectiveness of PEN solution for MPN.

Extended from Table 3, Fig. 5 shows the generalization performance of MPN when evaluated using attack data with different attack strengths. We observe that in-distribution generalization (corresponding to the same attack strength

Table 4. In-distribution generalization performance (testing accuracy, %) of MPN given different choices of VMs and datasets, attack types/strengths, and MPN input data formats ( $\mathbf{x}'$ ,  $\delta_{\text{PEN}}$ , and  $\delta$ ).

| Attack type       | Attack strength     | Dataset and victim model |                       |          |                   |                       |          |                   |                       |          |                |                       |          |                |                       |          |                   |                       |          |                        |                       |          |  |  |  |
|-------------------|---------------------|--------------------------|-----------------------|----------|-------------------|-----------------------|----------|-------------------|-----------------------|----------|----------------|-----------------------|----------|----------------|-----------------------|----------|-------------------|-----------------------|----------|------------------------|-----------------------|----------|--|--|--|
|                   |                     | CIFAR-10 ResNet9         |                       |          | CIFAR-10 ResNet18 |                       |          | CIFAR-10 ResNet20 |                       |          | CIFAR-10 VGG11 |                       |          | CIFAR-10 VGG13 |                       |          | CIFAR-100 ResNet9 |                       |          | Tiny-ImageNet ResNet18 |                       |          |  |  |  |
|                   |                     | $\mathbf{x}'$            | $\delta_{\text{PEN}}$ | $\delta$ | $\mathbf{x}'$     | $\delta_{\text{PEN}}$ | $\delta$ | $\mathbf{x}'$     | $\delta_{\text{PEN}}$ | $\delta$ | $\mathbf{x}'$  | $\delta_{\text{PEN}}$ | $\delta$ | $\mathbf{x}'$  | $\delta_{\text{PEN}}$ | $\delta$ | $\mathbf{x}'$     | $\delta_{\text{PEN}}$ | $\delta$ | $\mathbf{x}'$          | $\delta_{\text{PEN}}$ | $\delta$ |  |  |  |
| FGSM              | $\epsilon = 4/255$  | 60.13                    | 85.25                 | 96.82    | 60.00             | 86.92                 | 97.66    | 62.41             | 88.91                 | 97.64    | 47.42          | 73.40                 | 91.75    | 66.28          | 90.02                 | 98.57    | 57.99             | 82.22                 | 94.86    | 37.23                  | 84.27                 | 97.04    |  |  |  |
|                   | $\epsilon = 8/255$  | 78.80                    | 94.15                 | 96.89    | 80.44             | 95.49                 | 97.61    | 82.29             | 95.90                 | 97.72    | 63.13          | 86.76                 | 92.41    | 84.92          | 96.91                 | 98.66    | 75.58             | 91.65                 | 94.96    | 70.29                  | 91.17                 | 97.05    |  |  |  |
|                   | $\epsilon = 12/255$ | 86.49                    | 95.96                 | 96.94    | 88.03             | 96.89                 | 97.68    | 88.71             | 97.13                 | 97.81    | 73.71          | 90.19                 | 92.66    | 91.21          | 98.10                 | 98.71    | 82.27             | 94.01                 | 95.55    | 76.00                  | 93.45                 | 97.02    |  |  |  |
|                   | $\epsilon = 16/255$ | 90.16                    | 96.43                 | 96.94    | 91.71             | 97.34                 | 97.68    | 91.84             | 97.47                 | 97.79    | 79.51          | 91.28                 | 92.60    | 94.22          | 98.44                 | 98.73    | 86.50             | 94.04                 | 94.74    | 79.63                  | 94.35                 | 96.87    |  |  |  |
| PGD $\ell_\infty$ | $\epsilon = 4/255$  | 50.54                    | 76.43                 | 96.02    | 56.94             | 79.45                 | 96.96    | 55.01             | 80.05                 | 97.49    | 39.33          | 66.38                 | 91.84    | 57.12          | 81.18                 | 98.29    | 42.27             | 72.62                 | 92.65    | 35.48                  | 76.56                 | 97.18    |  |  |  |
|                   | $\epsilon = 8/255$  | 66.62                    | 83.20                 | 95.07    | 73.29             | 87.29                 | 95.38    | 67.49             | 86.19                 | 96.18    | 56.62          | 81.14                 | 92.78    | 69.16          | 88.46                 | 97.22    | 59.71             | 79.55                 | 90.43    | 61.85                  | 82.90                 | 96.05    |  |  |  |
|                   | $\epsilon = 12/255$ | 76.65                    | 89.73                 | 94.91    | 81.73             | 91.67                 | 95.55    | 76.41             | 90.16                 | 95.67    | 70.56          | 88.92                 | 94.13    | 78.67          | 92.93                 | 97.26    | 70.86             | 85.31                 | 91.28    | 73.82                  | 88.80                 | 96.38    |  |  |  |
|                   | $\epsilon = 16/255$ | 75.58                    | 86.95                 | 91.28    | 82.46             | 90.19                 | 93.19    | 76.58             | 87.79                 | 92.50    | 72.13          | 87.23                 | 91.85    | 78.28          | 90.20                 | 94.66    | 71.29             | 82.35                 | 86.84    | 73.19                  | 85.02                 | 93.54    |  |  |  |
| PGD $\ell_2$      | $\epsilon = 0.25$   | 36.75                    | 62.20                 | 99.66    | 46.35             | 70.17                 | 99.74    | 48.24             | 77.22                 | 99.75    | 36.47          | 45.17                 | 98.52    | 35.81          | 70.62                 | 99.85    | 35.92             | 61.91                 | 99.29    | 35.55                  | 35.68                 | 99.68    |  |  |  |
|                   | $\epsilon = 0.5$    | 53.42                    | 82.58                 | 99.64    | 60.89             | 84.70                 | 99.56    | 61.62             | 89.11                 | 99.61    | 41.56          | 66.58                 | 98.68    | 57.83          | 87.64                 | 99.83    | 48.89             | 79.26                 | 99.01    | 35.52                  | 54.56                 | 99.71    |  |  |  |
|                   | $\epsilon = 0.75$   | 62.66                    | 89.04                 | 99.48    | 71.01             | 89.89                 | 99.22    | 70.76             | 92.06                 | 99.36    | 47.02          | 78.12                 | 98.52    | 72.76          | 92.32                 | 99.74    | 59.19             | 85.14                 | 98.61    | 35.56                  | 81.33                 | 99.71    |  |  |  |
|                   | $\epsilon = 1$      | 71.65                    | 91.73                 | 99.26    | 77.09             | 92.09                 | 98.94    | 76.84             | 92.82                 | 98.96    | 54.20          | 84.30                 | 98.41    | 79.93          | 93.96                 | 99.57    | 66.97             | 87.63                 | 97.89    | 43.48                  | 88.81                 | 99.64    |  |  |  |
| CW                | $c = 0.1$           | 33.77                    | 55.60                 | 96.71    | 47.77             | 63.26                 | 96.11    | 33.56             | 63.11                 | 94.10    | 33.73          | 48.90                 | 94.37    | 33.68          | 65.48                 | 96.95    | 34.41             | 46.47                 | 92.55    | 35.96                  | 35.77                 | 95.52    |  |  |  |
|                   | $c = 1$             | 35.42                    | 64.46                 | 96.66    | 45.75             | 65.25                 | 97.45    | 33.74             | 62.71                 | 97.08    | 33.89          | 55.61                 | 91.29    | 36.12          | 68.66                 | 98.58    | 34.25             | 55.18                 | 93.25    | 35.54                  | 35.29                 | 89.35    |  |  |  |
|                   | $c = 10$            | 36.38                    | 64.45                 | 96.64    | 45.83             | 65.32                 | 97.41    | 33.83             | 63.52                 | 97.11    | 38.29          | 56.83                 | 91.33    | 38.51          | 68.28                 | 98.62    | 34.25             | 55.89                 | 93.18    | 35.45                  | 53.18                 | 94.20    |  |  |  |

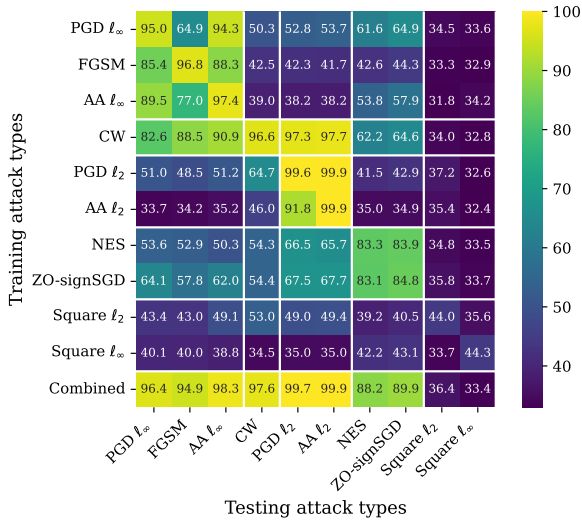


Figure 6. Model parsing accuracy (%) of MPN when trained on a row-specific attack type but evaluated on a column-specific attack type. The attack generation and data-model setups are consistent with Table 3. MPN takes adversarial perturbations as input. ‘Combined’ represents MPN trained on multiple attack types: PGD  $\ell_\infty$ , PGD  $\ell_2$ , CW, and ZO-signSGD.

for the train-time and test-time attacks) is easier to achieve than OOD generalization (different attack strengths at test time and train time). Another observation is that a smaller gap between the train-time attack strength and the test-time strength leads to better generalization performance.

Extended from Table 3 and Fig. 5 that focused on model parsing of adversarial attacks by fixing the VM architecture to ResNet9 on CIFAR-10, Table 4 shows the generalization of MPN under diverse setups of victim model architectures and datasets. The insights into model parsing are consistent with Table 3: (1) The use of true adversarial perturbations ( $\delta$ ) and PEN-estimated perturbations ( $\delta_{\text{PEN}}$ ) can yield higher model parsing accuracy; (2) Inferring model attributes from perfect-knowledge, gradient-based adversarial perturbations is easier, as supported by its over 90% testing accuracy; And (3) the model parsing accuracy gets better if adversarial attacks have a higher attack strength ( $\epsilon$ ).

**OOD generalization of MPN is difficult vs. unseen attack types at test time.** In Fig. 6, we present the model parsing accuracy of MPN when trained under one attack type (e.g., PGD  $\ell_\infty$  attack at row 1) but tested under another attack type (e.g., FGSM attack at column 2) on CIFAR-10. The diagonal entries of the matrix correspond to the in-distribution generalization of MPN given the attack type, while the off-diagonal entries denote OOD generalization when test-time attack types are different from train-time ones.

**First**, we find that MPN generalizes better across attack types when they share similarities, leading to the following *generalization communities*:  $\ell_\infty$  attacks (PGD  $\ell_\infty$ , FGSM, and AA  $\ell_\infty$ ),  $\ell_2$  attacks (CW, PGD  $\ell_2$ , or AA  $\ell_2$ ), and ZOO-based restricted-knowledge attacks (NES and ZO-signSGD). **Second**, Square attacks are difficult to learn and generalize, as evidenced by the low test accuracies in the last two rows and the last two columns. This is also consistent with Table 3. **Third**, given the existence of generalization communities, we then combine diverse attack types (including PGD  $\ell_\infty$ , PGD  $\ell_2$ , CW, and ZO-signSGD) into an augmented MPN training set and investigate if such a data augmentation can boost the OOD generalization of MPN. The results are summarized in the ‘**combined**’ row of Fig. 6. As we expect, the use of combined attack types indeed makes MPN generalize better across all attack types except for the random search-based Square attack.

In Fig. A1 of Appendix B, we find the consistent OOD generalization performance of MPN when PEN-based adversarial perturbations are used in MPN. In Fig. A2 of Appendix C, we peer into the generalization of MPN across various VM architectures (i.e., AT in Table 1), while maintaining configurations for other attributes (KS, AF, and WS). The observed performance is consistent with Fig. 6.

**MPN to uncover real VM attributes of transfer attacks.** As a use case of model parsing, we next investigate if MPN can correctly infer the source VM attributes from transfer attacks when applied to attacking a different model as shown in Fig. 2. Given the VM architecture ResNet9, we vary the

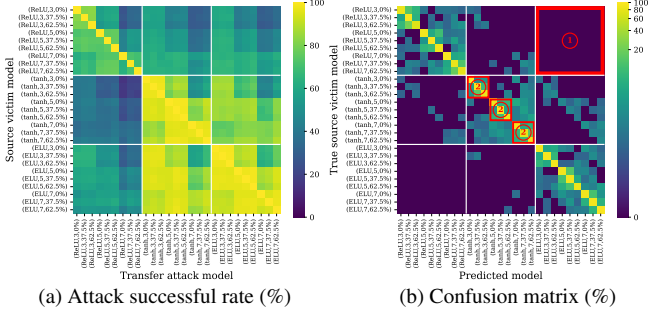


Figure 7. Model parsing of transfer attacks: Transfer attack success rate matrix (a) and model parsing confusion matrix (b). Given the architecture type ResNet9, the dataset CIFAR-10, and the attack type PGD  $\ell_\infty$  (with strength  $\epsilon = 8/255$ ), each model attribute combination (AF, KS, WS) defines a model instance to be attacked, transferred, or parsed.

values of model attributes KS, AF, and WS to produce 27 ResNet9-type VMs. **Fig. 7** shows the transfer attack success rate (ASR) matrix (Fig. 7a) and the model parsing confusion matrix (Fig. 7b). Here the transfer attack type is given by PGD  $\ell_\infty$  attack with strength  $\epsilon = 8/255$  on CIFAR-10.

In **Fig. 7a**, the off-diagonal entries denote ASRs of transfer attacks from row-wise VMs to attacking column-wise target models. Adversarial attacks generated from ReLU-based VMs are typically more difficult to transfer to smooth activation function (ELU or tanh)-based target models. By contrast, given the values of AF and KS, attacks are easier to transfer across models with different weight sparsity.

**Fig. 7b** presents the confusion matrix of MPN trained on attack data generated from all 27 ResNet9-alike VMs. Each row of the confusion matrix represents the true VM used to generate the attack dataset, and each column corresponds to a predicted model attribute configuration. Thus, the diagonal entries and the off-diagonal entries in Fig. 7b represent the correct model parsing accuracy and the misclassification rate on the incorrectly predicted model attribute configuration. As we can see, attacks generated from ReLU-based VMs result in a low misclassification rate of MPN on ELU or tanh-based predictions (see the marked region ①). Meanwhile, a high misclassification occurs for MPN when evaluated on attack data corresponding to different values of WS (see the marked region ②). The above results, together with our insights into ASRs of transfer attacks in Fig. 7a, suggest a connection between transfer attack and model parsing: *If attacks are difficult (or easy) to transfer from the source model to the target model, then inferring the source model attributes from these attacks turns to be easy (or difficult)*. To elucidate the above phenomenon, our investigation extends to assessing attack transferability via input gradient correlation, which indicates that a high alignment of gradients between models enhances transferability [81]. As seen in Fig. A3 of Appendix D, we show that attacks which easily transfer across models are difficult to parse accurately due to their gradient features lacking distinctiveness.

## Defense inspired by model parsing.

Inspired by the MPN’s ability to infer source model attributes of transfer attacks (Fig. 7), we propose an adversarial defense scheme. This scheme alters the target model’s attributes to differ from those of the

source model, improving its robustness against transfer attacks. Our rationale is that a model can achieve improved robustness against transfer attacks if it has distinct attributes from the source model used to generate these attacks. **Fig. 7** shows the robust accuracy (RA) and standard accuracy (SA) of the above defense method. As we can see, without any defense, transfer attacks remain effective. However, robustness (measured by RA) increases when one attribute is modified, especially when altering the AF type. This is expected, as modifying activation functions has been shown to improve model robustness [82]. Furthermore, when all attributes are modifiable, the defense achieves the highest RA without compromising SA.

**Other experimental studies.** We examine the influence of adversarial robustness of VMs in the generalization performance of MPN; see Fig. A4 in Appendix E. We find that adversarial attacks against robust VMs is harder to parse VM attributes than attacks against standard VMs. The possible rationale is that attacks carry rich VM information in input gradients. Yet, robust models typically exhibit weaker input gradient norms compared to standard models [83]. Thus, robust models are harder to infer due to the low power of input gradients. Fig. A5 provides an empirical justification for this rationale. In Appendix F, we examine the influence of other factors like PGD steps, step sizes, and transfer attack strengths on the generalization performance of MPN.

## 6. Conclusion

We study model parsing from adversarial attacks to deduce attributes of victim models, with the development of model parsing network (MPN). Our exploration spanned both in-distribution and out-of-distribution scenarios, evaluating MPN against diverse attack methods and model configurations. Key determinants such as input format, backbone network, and attack characteristics were analyzed for their impact on model parsing. We elucidated the conditions under which victim model information can be extracted from adversarial attacks. Our study empowers defenders with an enhanced understanding of attack provenance.

Table 5. Performance (RA and SA) of model parsing-enabled adversarial defense against transfer attacks. Each row represents either no defense or a defense strategy involving the alteration of attacked model attributes (KS, AF, WS) to differ from the source model attributes used to generate transfer attacks. ✓(✗) denotes w/ (w/o) modification. The transfer attack configurations follow Fig. 7.

| Setting        | KS | AF | WS | RA (%)      | SA (%) |
|----------------|----|----|----|-------------|--------|
| No Defense     | ✗  | ✗  | ✗  | 0           | 90.7   |
| Change 1 Attr. | ✓  | ✗  | ✗  | 31.2        | 90.4   |
|                | ✗  | ✓  | ✗  | 50.1        | 91.7   |
|                | ✗  | ✗  | ✓  | 10.9        | 90.6   |
| Change 2 Attr. | ✓  | ✓  | ✗  | 63.3        | 91.1   |
|                | ✗  | ✓  | ✓  | 34.6        | 90.1   |
|                | ✓  | ✗  | ✓  | 51.5        | 91.8   |
| Change 3 Attr. | ✓  | ✓  | ✓  | <b>66.3</b> | 91.2   |

## 7. Acknowledgement

The work was supported by the DARPA RED program.

## References

- [1] Aleksander Madry, Aleksandar Makelov, Ludwig Schmidt, Dimitris Tsipras, and Adrian Vladu. Towards deep learning models resistant to adversarial attacks. *arXiv preprint arXiv:1706.06083*, 2017. 1, 2, 3, 4, 18
- [2] Christian Szegedy, Wojciech Zaremba, Ilya Sutskever, Joan Bruna, Dumitru Erhan, Ian Goodfellow, and Rob Fergus. Intriguing properties of neural networks. *arXiv preprint arXiv:1312.6199*, 2013. 1
- [3] Ian J Goodfellow, Jonathon Shlens, and Christian Szegedy. Explaining and harnessing adversarial examples. *arXiv preprint arXiv:1412.6572*, 2014. 1, 2, 3
- [4] Cihang Xie, Jianyu Wang, Zhishuai Zhang, Yuyin Zhou, Lingxi Xie, and Alan Yuille. Adversarial examples for semantic segmentation and object detection. In *Proceedings of the IEEE international conference on computer vision*, pages 1369–1378, 2017.
- [5] James Tu, Mengye Ren, Sivabalan Manivasagam, Ming Liang, Bin Yang, Richard Du, Frank Cheng, and Raquel Urtasun. Physically realizable adversarial examples for lidar object detection. In *Proceedings of the IEEE/CVF Conference on Computer Vision and Pattern Recognition*, pages 13716–13725, 2020.
- [6] Vegard Antun, Francesco Renna, Clarice Poon, Ben Adcock, and Anders C Hansen. On instabilities of deep learning in image reconstruction and the potential costs of ai. *Proceedings of the National Academy of Sciences*, 117(48):30088–30095, 2020.
- [7] Ankit Raj, Yoram Bresler, and Bo Li. Improving robustness of deep-learning-based image reconstruction. In *International Conference on Machine Learning*, pages 7932–7942. PMLR, 2020.
- [8] Ziyu Jiang, Tianlong Chen, Ting Chen, and Zhangyang Wang. Robust pre-training by adversarial contrastive learning. *Advances in neural information processing systems*, 33:16199–16210, 2020.
- [9] Lijie Fan, Sijia Liu, Pin-Yu Chen, Gaoyuan Zhang, and Chuang Gan. When does contrastive learning preserve adversarial robustness from pretraining to finetuning? *Advances in neural information processing systems*, 34:21480–21492, 2021.
- [10] Rishi Bommasani, Drew A Hudson, Ehsan Adeli, Russ Altman, Simran Arora, Sydney von Arx, Michael S Bernstein, Jeannette Bohg, Antoine Bosselut, Emma Brunskill, et al. On the opportunities and risks of foundation models. *arXiv preprint arXiv:2108.07258*, 2021.
- [11] Natalie Maus, Patrick Chao, Eric Wong, and Jacob Gardner. Adversarial prompting for black box foundation models. *arXiv preprint arXiv:2302.04237*, 2023. 1
- [12] Nicholas Carlini and David Wagner. Towards evaluating the robustness of neural networks. In *2017 IEEE Symposium on Security and Privacy (SP)*, pages 39–57. Ieee, 2017. 1, 2, 3, 4
- [13] Francesco Croce and Matthias Hein. Reliable evaluation of adversarial robustness with an ensemble of diverse parameter-free attacks. In *International conference on machine learning*, pages 2206–2216. PMLR, 2020. 1, 3, 4
- [14] Pin-Yu Chen, Huan Zhang, Yash Sharma, Jinfeng Yi, and Chao-Jui Hsieh. Zoo: Zeroth order optimization based black-box attacks to deep neural networks without training substitute models. In *Proceedings of the 10th ACM Workshop on Artificial Intelligence and Security*, pages 15–26. ACM, 2017. 1, 3
- [15] Sijia Liu, Pin-Yu Chen, Xiangyi Chen, and Mingyi Hong. signSGD via zeroth-order oracle. In *International Conference on Learning Representations*, 2019. 2, 3, 4
- [16] Andrew Ilyas, Logan Engstrom, Anish Athalye, and Jessy Lin. Black-box adversarial attacks with limited queries and information. In *International conference on machine learning*, pages 2137–2146. PMLR, 2018. 3, 4
- [17] Maksym Andriushchenko, Francesco Croce, Nicolas Flammarion, and Matthias Hein. Square attack: a query-efficient black-box adversarial attack via random search. In *Computer Vision—ECCV 2020: 16th European Conference, Glasgow, UK, August 23–28, 2020, Proceedings, Part XXIII*, pages 484–501. Springer, 2020. 1, 2, 3, 4
- [18] Cihang Xie, Zhishuai Zhang, Yuyin Zhou, Song Bai, Jianyu Wang, Zhou Ren, and Alan L Yuille. Improving transferability of adversarial examples with input diversity. In *Proceedings of the IEEE/CVF Conference on Computer Vision and Pattern Recognition*, pages 2730–2739, 2019. 1, 19
- [19] Chaowei Xiao, Jun-Yan Zhu, Bo Li, Warren He, Mingyan Liu, and Dawn Song. Spatially transformed adversarial examples. In *International Conference on Learning Representations*, 2018. URL <https://openreview.net/forum?id=HyydRMZC->. 2
- [20] Seyed-Mohsen Moosavi-Dezfooli, Alhussein Fawzi, and Pascal Frossard. Deepfool: a simple and accurate method to fool deep neural networks. In *Proceedings of the IEEE conference on computer vision and pattern recognition*, pages 2574–2582, 2016. 1
- [21] Wieland Brendel, Jonas Rauber, and Matthias Bethge. Decision-based adversarial attacks: Reliable attacks against black-box machine learning models. *arXiv preprint arXiv:1712.04248*, 2017. 1, 2, 3
- [22] Hongyang Zhang, Yaodong Yu, Jiantao Jiao, Eric P Xing, Laurent El Ghaoui, and Michael I Jordan. Theoretically principled trade-off between robustness and accuracy. *ICML*, 2019. 1, 2, 3

- [23] Eric Wong and J Zico Kolter. Provable defenses against adversarial examples via the convex outer adversarial polytope. *arXiv preprint arXiv:1711.00851*, 2017. 3
- [24] Hadi Salman, Mingjie Sun, Greg Yang, Ashish Kapoor, and J Zico Kolter. Denoised smoothing: A provable defense for pretrained classifiers. *NeurIPS*, 2020. 3
- [25] Eric Wong, Leslie Rice, and J Zico Kolter. Fast is better than free: Revisiting adversarial training. *arXiv preprint arXiv:2001.03994*, 2020. 3
- [26] Yair Carmon, Aditi Raghunathan, Ludwig Schmidt, John C Duchi, and Percy S Liang. Unlabeled data improves adversarial robustness. In *Advances in Neural Information Processing Systems (NeurIPS)*, 2019.
- [27] Ali Shafahi, Mahyar Najibi, Mohammad Amin Ghiasi, Zheng Xu, John Dickerson, Christoph Studer, Larry S Davis, Gavin Taylor, and Tom Goldstein. Adversarial training for free! In *Advances in Neural Information Processing Systems*, pages 3353–3364, 2019. 2, 3
- [28] Mo Zhou and Vishal M Patel. On trace of pgd-like adversarial attacks. *arXiv preprint arXiv:2205.09586*, 2022. 2, 3
- [29] Kathrin Grosse, Praveen Manoharan, Nicolas Papernot, Michael Backes, and Patrick McDaniel. On the (statistical) detection of adversarial examples. *arXiv preprint arXiv:1702.06280*, 2017.
- [30] Puyudi Yang, Jianbo Chen, Cho-Jui Hsieh, Jane-Ling Wang, and Michael Jordan. MI-loo: Detecting adversarial examples with feature attribution. In *Proceedings of the AAAI Conference on Artificial Intelligence (AAAI)*, 2020.
- [31] Jan Hendrik Metzen, Tim Genewein, Volker Fischer, and Bastian Bischoff. On detecting adversarial perturbations. *arXiv preprint arXiv:1702.04267*, 2017.
- [32] Dongyu Meng and Hao Chen. Magnet: a two-pronged defense against adversarial examples. In *Proceedings of the 2017 ACM SIGSAC Conference on Computer and Communications Security*, pages 135–147. ACM, 2017.
- [33] Bartosz Wójcik, Paweł Morawiecki, Marek Śmieja, Tomasz Krzyżek, Przemysław Spurek, and Jacek Tabor. Adversarial examples detection and analysis with layer-wise autoencoders. *arXiv preprint arXiv:2006.10013*, 2020. 2, 3
- [34] Changhao Shi, Chester Holtz, and Gal Mishne. Online adversarial purification based on self-supervision. *arXiv preprint arXiv:2101.09387*, 2021. 2, 3
- [35] Jongmin Yoon, Sung Ju Hwang, and Juho Lee. Adversarial purification with score-based generative models. In *International Conference on Machine Learning*, pages 12062–12072. PMLR, 2021.
- [36] Vignesh Srinivasan, Csaba Rohrer, Arturo Marban, Klaus-Robert Müller, Wojciech Samek, and Shinichi Nakajima. Robustifying models against adversarial attacks by langevin dynamics. *Neural Networks*, 137:1–17, 2021. 2, 3
- [37] Yihua Zhang, Guanhua Zhang, Prashant Khanduri, Mingyi Hong, Shiyu Chang, and Sijia Liu. Revisiting and advancing fast adversarial training through the lens of bi-level optimization. In *International Conference on Machine Learning*, pages 26693–26712. PMLR, 2022. 2, 3
- [38] Yimeng Zhang, Yuguang Yao, Jinghan Jia, Jinfeng Yi, Mingyi Hong, Shiyu Chang, and Sijia Liu. How to robustify black-box ML models? a zeroth-order optimization perspective. In *International Conference on Learning Representations*, 2022. 1
- [39] Sheng-Yu Wang, Oliver Wang, Richard Zhang, Andrew Owens, and Alexei A Efros. Cnn-generated images are surprisingly easy to spot... for now. In *Proceedings of the IEEE/CVF conference on computer vision and pattern recognition*, pages 8695–8704, 2020. 1, 2, 3
- [40] Vishal Asnani, Xi Yin, Tal Hassner, and Xiaoming Liu. Reverse engineering of generative models: Inferring model hyperparameters from generated images. *arXiv preprint arXiv:2106.07873*, 2021. 2, 3
- [41] Prafulla Dhariwal and Alexander Nichol. Diffusion models beat gans on image synthesis. *Advances in Neural Information Processing Systems*, 34:8780–8794, 2021.
- [42] Ning Yu, Larry S Davis, and Mario Fritz. Attributing fake images to gans: Learning and analyzing gan fingerprints. In *Proceedings of the IEEE/CVF international conference on computer vision*, pages 7556–7566, 2019. 2, 3
- [43] Joel Frank, Thorsten Eisenhofer, Lea Schönherr, Asja Fischer, Dorothea Kolossa, and Thorsten Holz. Leveraging frequency analysis for deep fake image recognition. In *International conference on machine learning*, pages 3247–3258. PMLR, 2020.
- [44] Luca Guarnera, Oliver Giudice, and Sebastiano Battiato. Deepfake detection by analyzing convolutional traces. In *Proceedings of the IEEE/CVF conference on computer vision and pattern recognition workshops*, pages 666–667, 2020. 2, 3
- [45] Tarik Dzanic, Karan Shah, and Freddie Witherden. Fourier spectrum discrepancies in deep network generated images. *Advances in neural information processing systems*, 33:3022–3032, 2020. 1
- [46] Fangzhou Liao, Ming Liang, Yinpeng Dong, Tianyu Pang, Xiaolin Hu, and Jun Zhu. Defense against Adversarial Attacks Using High-Level Representation Guided Denoiser. *arXiv:1712.02976 [cs]*, May 2018. 2, 3
- [47] Weili Nie, Brandon Guo, Yujia Huang, Chaowei Xiao, Arash Vahdat, and Anima Anandkumar. Diffusion models for adversarial purification. *arXiv preprint arXiv:2205.07460*, 2022. 2, 3
- [48] David Aaron Nicholson and Vincent Emanuele. Reverse engineering adversarial attacks with fingerprints from adversarial examples. *arXiv preprint arXiv:2301.13869*, 2023. 2, 3

- [49] Yifan Gong, Yuguang Yao, Yize Li, Yimeng Zhang, Xiaoming Liu, Xue Lin, and Sijia Liu. Reverse engineering of imperceptible adversarial image perturbations. *arXiv preprint arXiv:2203.14145*, 2022. 2, 3, 6
- [50] Xiawei Wang, Yao Li, Cho-Jui Hsieh, and Thomas Chun Man Lee. CAN MACHINE TELL THE DISTORTION DIFFERENCE? a REVERSE ENGINEERING STUDY OF ADVERSARIAL ATTACKS, 2023. URL <https://openreview.net/forum?id=NdFKHCFxXjS>. 2, 3
- [51] Michael Goebel, Jason Bunk, Srinjoy Chattopadhyay, Lakshmanan Nataraj, Shivkumar Chandrasekaran, and BS Manjunath. Attribution of gradient based adversarial attacks for reverse engineering of deceptions. *arXiv preprint arXiv:2103.11002*, 2021. 2, 3
- [52] Hossein Souri, Pirazh Khorramshahi, Chun Pong Lau, Micah Goldblum, and Rama Chellappa. Identification of attack-specific signatures in adversarial examples. *arXiv preprint arXiv:2110.06802*, 2021.
- [53] Darshan Thaker, Paris Giampouras, and René Vidal. Reverse engineering  $\ell_p$  attacks: A block-sparse optimization approach with recovery guarantees. In *International Conference on Machine Learning*, pages 21253–21271. PMLR, 2022. 2, 3
- [54] Zhongyi Guo, Keji Han, Yao Ge, Wei Ji, and Yun Li. Scalable attribution of adversarial attacks via multi-task learning. *arXiv preprint arXiv:2302.14059*, 2023. 2, 3
- [55] Pratyush Maini, Xinyun Chen, Bo Li, and Dawn Song. Perturbation type categorization for multiple  $\ell_p$  bounded adversarial robustness, 2021. URL <https://openreview.net/forum?id=Oe2XI-Aft-k>. 2, 3
- [56] Defense Advanced Research Projects Agency (DARPA). Reverse engineering of deceptions. <https://www.darpa.mil/program/reverse-engineering-of-deceptions>, 2023. Accessed: 2024-02-28. 2
- [57] Kaidi Xu, Sijia Liu, Pu Zhao, Pin-Yu Chen, Huan Zhang, Quanfu Fan, Deniz Erdogmus, Yanzhi Wang, and Xue Lin. Structured adversarial attack: Towards general implementation and better interpretability. In *ICLR*, 2019. 2
- [58] Pin-Yu Chen, Yash Sharma, Huan Zhang, Jinfeng Yi, and Cho-Jui Hsieh. EAD: elastic-net attacks to deep neural networks via adversarial examples. In *Proceedings of the AAAI Conference on Artificial Intelligence*, pages 10–17, 2018.
- [59] Minhao Cheng, Simranjit Singh, Patrick Chen, Pin-Yu Chen, Sijia Liu, and Cho-Jui Hsieh. Sign-opt: A query-efficient hard-label adversarial attack. *arXiv preprint arXiv:1909.10773*, 2019. 3
- [60] Jinghui Chen and Quanquan Gu. Rays: A ray searching method for hard-label adversarial attack. In *Proceedings of the 26th ACM SIGKDD International Conference on Knowledge Discovery & Data Mining*, pages 1739–1747, 2020. 2, 3
- [61] K. Eykholt, I. Evtimov, E. Fernandes, B. Li, A. Rahmati, C. Xiao, A. Prakash, T. Kohno, and D. Song. Robust physical-world attacks on deep learning visual classification. In *Proceedings of the Conference on Computer Vision and Pattern Recognition (CVPR)*, 2018. 2
- [62] Juncheng Li, Frank Schmidt, and Zico Kolter. Adversarial camera stickers: A physical camera-based attack on deep learning systems. In *International Conference on Machine Learning*, pages 3896–3904, 2019.
- [63] A. Athalye, L. Engstrom, A. Ilyas, and K. Kwok. Synthesizing robust adversarial examples. In *ICML*, 2018.
- [64] Shang-Tse Chen, Cory Cornelius, Jason Martin, and Duen Horng Polo Chau. Shapeshifter: Robust physical adversarial attack on faster r-cnn object detector. In *Joint European Conference on Machine Learning and Knowledge Discovery in Databases*, pages 52–68. Springer, 2018.
- [65] Kaidi Xu, Gaoyuan Zhang, Sijia Liu, Quanfu Fan, Mengshu Sun, Hongge Chen, Pin-Yu Chen, Yanzhi Wang, and Xue Lin. Evading real-time person detectors by adversarial t-shirt. *arXiv preprint arXiv:1910.11099*, 2019.
- [66] Donghua Wang, Wen Yao, Tingsong Jiang, Guijiang Tang, and Xiaoqian Chen. A survey on physical adversarial attack in computer vision. *arXiv preprint arXiv:2209.14262*, 2022. 2
- [67] Kaidi Xu, Sijia Liu, Gaoyuan Zhang, Mengshu Sun, Pu Zhao, Quanfu Fan, Chuang Gan, and Xue Lin. Interpreting adversarial examples by activation promotion and suppression. *arXiv preprint arXiv:1904.02057*, 2019. 3
- [68] Gaoyuan Zhang, Songtao Lu, Yihua Zhang, Xiangyi Chen, Pin-Yu Chen, Quanfu Fan, Lee Martie, Lior Horeish, Mingyi Hong, and Sijia Liu. Distributed adversarial training to robustify deep neural networks at scale. In *Uncertainty in Artificial Intelligence*, pages 2353–2363. PMLR, 2022. 3
- [69] Akhilan Boopathy, Lily Weng, Sijia Liu, Pin-Yu Chen, Gaoyuan Zhang, and Luca Daniel. Fast training of provably robust neural networks by singleprop. In *Proceedings of the AAAI Conference on Artificial Intelligence*, pages 6803–6811, 2021. 3
- [70] Aditi Raghunathan, Jacob Steinhardt, and Percy Liang. Certified defenses against adversarial examples. In *International Conference on Learning Representations*, 2018. URL <https://openreview.net/forum?id=Bys4ob-Rb>. 3
- [71] Hadi Salman, Jerry Li, Ilya Razenshteyn, Pengchuan Zhang, Huan Zhang, Sebastian Bubeck, and Greg Yang. Provably robust deep learning via adversarially trained smoothed classifiers. *Advances in Neural Information Processing Systems*, 32, 2019. 3
- [72] Jeremy Cohen, Elan Rosenfeld, and Zico Kolter. Certified adversarial robustness via randomized smoothing. In *international conference on machine learning*, pages 1310–1320. PMLR, 2019. 3

- [73] Seong Joon Oh, Bernt Schiele, and Mario Fritz. Towards reverse-engineering black-box neural networks. *Explainable AI: Interpreting, Explaining and Visualizing Deep Learning*, pages 121–144, 2019. 3
- [74] Binghui Wang and Neil Zhenqiang Gong. Stealing hyperparameters in machine learning. In *2018 IEEE symposium on security and privacy (SP)*, pages 36–52. IEEE, 2018. 3
- [75] Sijia Liu, Pin-Yu Chen, Bhavya Kailkhura, Gaoyuan Zhang, Alfred O Hero III, and Pramod K Varshney. A primer on zeroth-order optimization in signal processing and machine learning: Principals, recent advances, and applications. *IEEE Signal Processing Magazine*, 37(5):43–54, 2020. 4
- [76] Song Han, Jeff Pool, John Tran, and William Dally. Learning both weights and connections for efficient neural network. *Advances in neural information processing systems*, 28, 2015. 4
- [77] Jonathan Frankle and Michael Carbin. The lottery ticket hypothesis: Finding sparse, trainable neural networks. *arXiv preprint arXiv:1803.03635*, 2018. 4, 13
- [78] Yann LeCun, Yoshua Bengio, and Geoffrey Hinton. Deep learning. *nature*, 521(7553):436–444, 2015. 5
- [79] Oriol Vinyals, Charles Blundell, Timothy Lillicrap, Daan Wierstra, et al. Matching networks for one shot learning. *Advances in neural information processing systems*, 29, 2016. 5
- [80] Kai Zhang, Wangmeng Zuo, Yunjin Chen, Deyu Meng, and Lei Zhang. Beyond a gaussian denoiser: Residual learning of deep cnn for image denoising. *IEEE transactions on image processing*, 26(7):3142–3155, 2017. 6
- [81] Ambra Demontis, Marco Melis, Maura Pintor, Matthew Jagielski, Battista Biggio, Alina Oprea, Cristina Nita-Rotaru, and Fabio Roli. Why do adversarial attacks transfer? explaining transferability of evasion and poisoning attacks. In *28th USENIX security symposium (USENIX security 19)*, pages 321–338, 2019. 8
- [82] Cihang Xie, Mingxing Tan, Boqing Gong, Alan Yuille, and Quoc V Le. Smooth adversarial training. *arXiv preprint arXiv:2006.14536*, 2020. 8
- [83] Chris Finlay and Adam M Oberman. Scaleable input gradient regularization for adversarial robustness. *Machine Learning with Applications*, 3:100017, 2021. 8
- [84] Xiaolong Ma, Geng Yuan, Xuan Shen, Tianlong Chen, Xuxi Chen, Xiaohan Chen, Ning Liu, Minghai Qin, Sijia Liu, Zhangyang Wang, et al. Sanity checks for lottery tickets: Does your winning ticket really win the jackpot? *Advances in Neural Information Processing Systems*, 34:12749–12760, 2021. 13
- [85] Guillaume Leclerc, Andrew Ilyas, Logan Engstrom, Sung Min Park, Hadi Salman, and Aleksander Madry. FFCV: Accelerating training by removing data bottlenecks, 2023. URL <https://openreview.net/forum?id=Ew9gIwAQ7wr>. 13
- [86] Yinpeng Dong, Fangzhou Liao, Tianyu Pang, Hang Su, Jun Zhu, Xiaolin Hu, and Jianguo Li. Boosting adversarial attacks with momentum. In *Proceedings of the IEEE conference on computer vision and pattern recognition*, pages 9185–9193, 2018. 19

# Appendix

## A. Victim model training, evaluation, and attack setups

When training all CIFAR-10, CIFAR-100, and Tiny-ImageNet victim models (each of which is given by an attribute combination), we use the SGD optimizer with the cosine annealing learning rate schedule and an initial learning rate of 0.1. The weight decay is  $5e-4$ , and the batch size is 256. The number of training epochs is 75 for CIFAR-10 and CIFAR-100, and 100 for Tiny-ImageNet. When the weight sparsity (WS) is promoted, we follow the one-shot magnitude pruning method [77, 84] to obtain a sparse model. To obtain models with different activation functions (AF) and kernel sizes (KS), we modify the convolutional block design in the ResNet and VGG model family accordingly from 3, ReLU to others, *i.e.*, 5/7, tanh/ELU. Table A1 shows the testing accuracy (%) of victim models on different datasets, given any studied (AF, KS, WS) tuple included in Table 2. It is worth noting that we accelerate victim model training by using FFCV [85] when loading the dataset.

Table A1. Victim model performance (testing accuracy, %) given different choices of datasets and model architectures.

| Dataset       | AT       | Attribute combination |       |       |        |       |       |      |       |       |      |       |       |        |       |       |      |       |       |      |       |       |       |       |       |
|---------------|----------|-----------------------|-------|-------|--------|-------|-------|------|-------|-------|------|-------|-------|--------|-------|-------|------|-------|-------|------|-------|-------|-------|-------|-------|
|               |          | 3                     |       |       | ReLU 5 |       |       | 7    |       |       | 3    |       |       | tanh 5 |       |       | 7    |       |       | 3    |       |       | ELU 5 |       |       |
|               |          | 0%                    | 37.5% | 62.5% | 0%     | 37.5% | 62.5% | 0%   | 37.5% | 62.5% | 0%   | 37.5% | 62.5% | 0%     | 37.5% | 62.5% | 0%   | 37.5% | 62.5% | 0%   | 37.5% | 62.5% | 0%    | 37.5% | 62.5% |
| CIFAR-10      | ResNet9  | 94.4                  | 93.9  | 94.2  | 93.3   | 93.5  | 93.5  | 92.4 | 92.8  | 92.8  | 89.0 | 88.8  | 89.9  | 88.4   | 88.6  | 88.2  | 87.0 | 87.2  | 88.0  | 91.0 | 91.2  | 90.7  | 90.3  | 90.2  | 90.5  |
|               | ResNet18 | 94.7                  | 94.9  | 95.0  | 94.2   | 94.5  | 94.5  | 93.9 | 93.5  | 93.6  | 87.1 | 87.5  | 88.2  | 84.2   | 84.9  | 85.5  | 81.3 | 81.2  | 85.1  | 90.6 | 90.8  | 90.6  | 90.1  | 91.1  | 90.5  |
|               | ResNet20 | 92.1                  | 92.5  | 92.3  | 92.0   | 92.2  | 92.0  | 90.9 | 91.8  | 91.5  | 89.7 | 89.7  | 89.7  | 89.5   | 89.4  | 89.6  | 88.3 | 88.2  | 88.9  | 90.7 | 91.2  | 90.9  | 90.3  | 90.5  | 90.6  |
|               | VGG11    | 91.0                  | 91.1  | 90.4  | 89.8   | 89.9  | 89.4  | 88.2 | 88.4  | 88.0  | 88.7 | 89.1  | 88.9  | 87.2   | 87.6  | 87.6  | 87.0 | 86.8  | 87.0  | 89.4 | 89.5  | 89.5  | 88.0  | 88.2  | 88.5  |
|               | VGG13    | 93.1                  | 93.3  | 93.0  | 92.0   | 92.2  | 92.6  | 91.2 | 91.1  | 91.0  | 90.1 | 90.1  | 89.3  | 89.1   | 89.3  | 88.2  | 88.8 | 88.8  | 90.8  | 90.9 | 90.8  | 89.2  | 89.5  | 89.4  | 88.7  |
| CIFAR-100     | ResNet9  | 73.3                  | 73.6  | 73.5  | 71.8   | 71.9  | 71.2  | 69.1 | 69.8  | 69.2  | 58.6 | 60.1  | 60.3  | 60.1   | 61.2  | 62.0  | 58.2 | 59.8  | 60.3  | 70.8 | 70.7  | 70.8  | 69.5  | 69.6  | 69.8  |
|               | ResNet18 | 74.4                  | 75.0  | 75.6  | 73.6   | 73.0  | 74.6  | 71.2 | 71.0  | 70.9  | 62.0 | 62.0  | 62.9  | 57.3   | 59.3  | 60.1  | 51.3 | 53.4  | 57.1  | 70.1 | 70.8  | 71.1  | 66.8  | 69.7  | 69.7  |
|               | ResNet20 | 68.3                  | 68.4  | 67.5  | 67.8   | 67.5  | 67.7  | 66.8 | 66.7  | 67.6  | 59.9 | 61.3  | 59.6  | 61.9   | 62.0  | 62.1  | 59.9 | 61.2  | 61.2  | 66.4 | 67.6  | 67.7  | 67.0  | 67.3  | 67.2  |
|               | VGG11    | 68.3                  | 68.4  | 67.7  | 65.2   | 65.7  | 65.8  | 62.4 | 62.0  | 62.6  | 65.2 | 65.5  | 65.5  | 63.6   | 63.6  | 63.9  | 62.1 | 61.8  | 62.5  | 66.2 | 66.5  | 65.9  | 64.6  | 64.0  | 61.5  |
|               | VGG13    | 71.0                  | 70.6  | 71.1  | 69.9   | 70.5  | 70.3  | 66.5 | 66.5  | 67.2  | 66.7 | 67.5  | 67.5  | 65.2   | 65.5  | 67.1  | 63.9 | 63.4  | 65.0  | 68.9 | 69.3  | 69.5  | 66.3  | 66.7  | 67.1  |
| Tiny-ImageNet | ResNet18 | 63.7                  | 64.1  | 63.5  | 61.5   | 62.7  | 62.6  | 59.6 | 61.0  | 61.7  | 47.0 | 48.1  | 50.0  | 46.6   | 47.9  | 48.3  | 41.0 | 43.5  | 44.6  | 57.2 | 57.9  | 58.1  | 52.7  | 53.8  | 53.6  |

For different attack types, we list all the attack configurations below:

- ◆ FGSM. We set the attack strength  $\epsilon$  equal to  $4/255$ ,  $8/255$ ,  $12/255$ , and  $16/255$ , respectively.
- ◆ PGD  $\ell_\infty$ . We set the attack step number equal to 10, and the attack strength-learning rate combinations as ( $\epsilon = 4/255$ ,  $\alpha = 0.5/255$ ), ( $\epsilon = 8/255$ ,  $\alpha = 1/255$ ), ( $\epsilon = 12/255$ ,  $\alpha = 2/255$ ), and ( $\epsilon = 16/255$ ,  $\alpha = 2/255$ ).
- ◆ PGD  $\ell_2$ . We set the step number equal to 10, and the attack strength-learning rate combinations as ( $\epsilon = 0.25$ ,  $\alpha = 0.05$ ), ( $\epsilon = 0.5$ ,  $\alpha = 0.1$ ), ( $\epsilon = 0.75$ ,  $\alpha = 0.15$ ), and ( $\epsilon = 1.0$ ,  $\alpha = 0.2$ ).
- ◆ CW. We use  $\ell_2$  version CW attack with the attack conference parameter  $\kappa$  equal to 0. We also set the learning rate equal to 0.01 and the maximum iteration number equal to 50 to search for successful attacks.
- ◆ AutoAttack  $\ell_\infty$ . We use the standard version of AutoAttack with the  $\ell_\infty$  norm and  $\epsilon$  equal to  $4/255$ ,  $8/255$ ,  $12/255$ , and  $16/255$ , respectively.
- ◆ AutoAttack  $\ell_2$ . We use the standard version of AutoAttack with the  $\ell_2$  norm and  $\epsilon$  equal to 0.25, 0.5, 0.75, and 1.0, respectively.
- ◆ SquareAttack  $\ell_\infty$ . We set the maximum query number equal to 5000 with  $\ell_\infty$  norm  $\epsilon$  equal to  $4/255$ ,  $8/255$ ,  $12/255$ , and  $16/255$ , respectively.
- ◆ SquareAttack  $\ell_2$ . We set the maximum query number equal to 5000 with  $\ell_\infty$  norm  $\epsilon$  equal to 0.25, 0.5, 0.75, and 1.0, respectively.
- ◆ NES. We set the query number for each gradient estimate equal to 10, together with  $\mu = 0.01$  (*i.e.*, the value of the smoothing parameter to obtain the finite difference of function evaluations). We also set the learning rate by 0.0005, and the maximum iteration number by 500 for each adversarial example generation.
- ◆ ZO-signSGD. We set the query number for each gradient estimate equal to 10 with  $\mu = 0.01$ . We also set the learning rate equal to 0.0005, and the maximum iteration number equal to 500 for each adversarial example generation. The only difference between ZO-signSGD and NES is the gradient estimation method in ZOO. ZO-signSGD uses the sign of forward difference-based estimator while NES uses the central difference-based estimator.

## B. OOD generalization performance of MPN across attack types when PEN is used

Similar to Fig. 7, Fig. A1 shows the generalization performance of MPN when trained on a row-specific attack type but evaluated on a column-specific attack type when  $\delta_{\text{PEN}}$  is given as input. When MPN is trained on the collection of four attack types PGD  $\ell_\infty$ , PGD  $\ell_2$ , CW, and ZO-signSGD (*i.e.*, the ‘Combined’ row), such a data augmentation can boost the OOD generalization except for the random search-based Square attack.

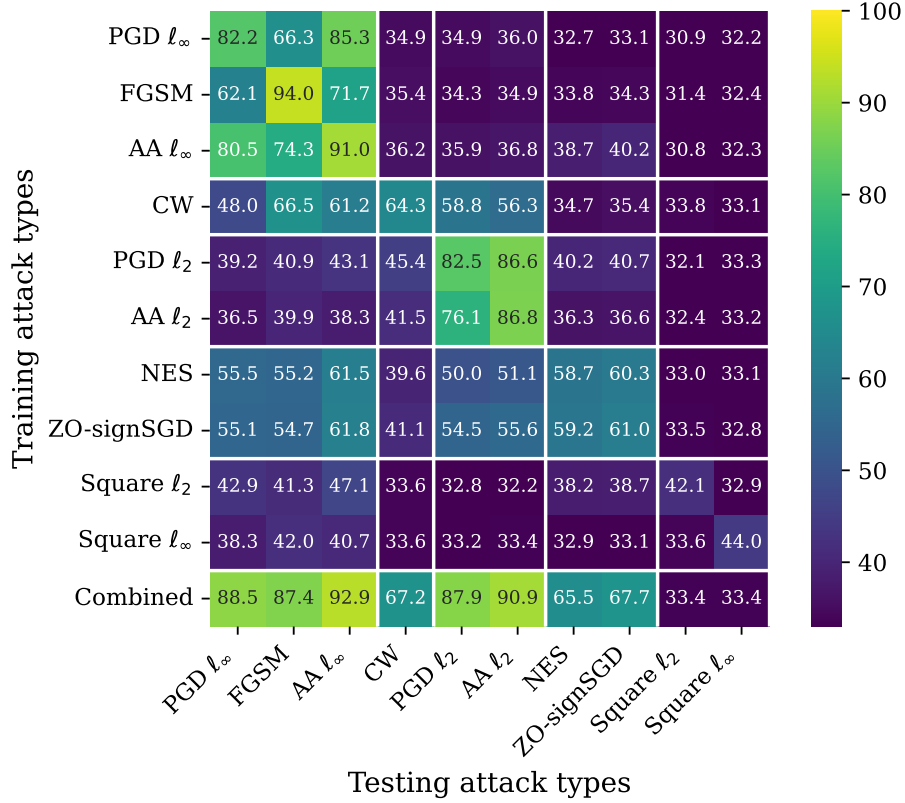


Figure A1. Generalization performance matrix of MPN when trained on a row-specific attack type but evaluated on a column-specific attack type given  $\delta_{\text{PEN}}$  as input. The attack data are given by adversarial perturbations with strength  $\epsilon = 8/255$  for  $\ell_\infty$  attacks,  $\epsilon = 0.5$  for  $\ell_2$  attacks, and  $c = 1$  for CW attack. The victim model architecture and the dataset are set as ResNet9 and CIFAR-10. The ‘combined’ row represents MPN training on the collection of four attack types: PGD  $\ell_\infty$ , PGD  $\ell_2$ , CW, and ZO-signSGD.

### C. MPN across different architecture types (AT)

We also peer into the generalization of MPN across different VM architectures (*i.e.*, AT in Table 1), while maintaining constant configurations for other attributes (KS, AF, and WS).

Fig. A2 demonstrates the generalization matrix of MPN when trained and evaluated using adversarial perturbations generated from different VM architectures (*i.e.*, different values of AT in Table 1) by fixing the configurations of other attributes (KS, AF, and WS). We observe that given an attack type, the in-distribution MPN generalization remains well across VM architectures. Yet, the OOD generalization of MPN (corresponding to the off-diagonal entries of the generalization matrix) rapidly degrades if the test-time VM architecture is different from the train-time one. This inspires us to train MPN on more AT variants in order to retain the model parsing performance, as shown in the last row of each subfigure of Fig. A2.

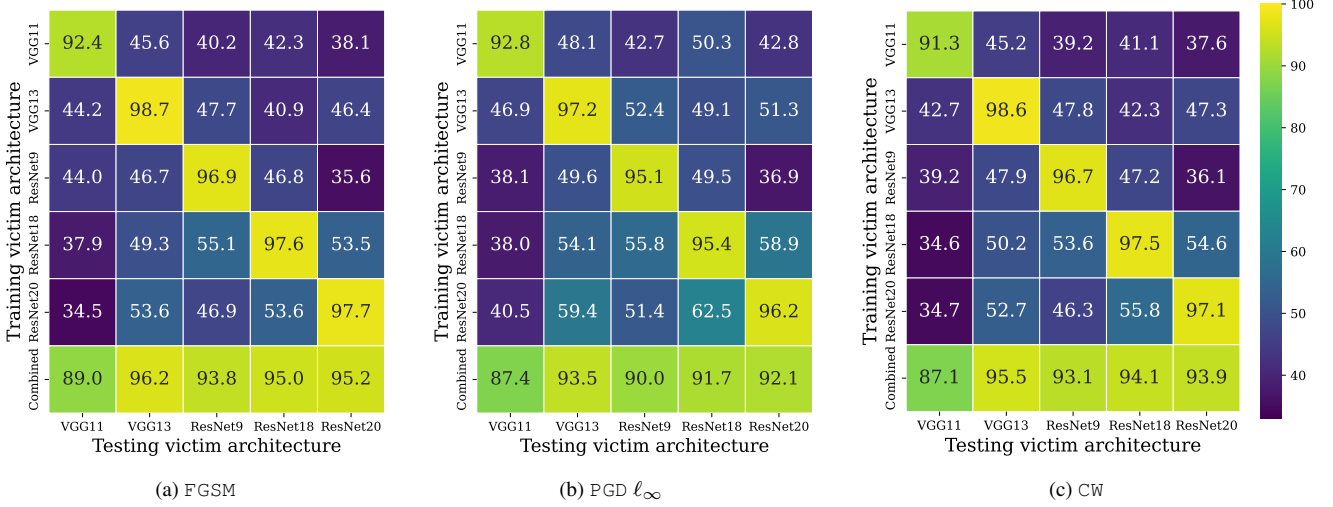


Figure A2. Generalization matrix (%) of MPN when trained on attack data generated from a row-specific architecture but evaluated on attack data generated from a column-specific architecture. Both the train-time and test-time architectures share the same VM attributes in KS, AF, and WS. The attack type is specified by FGSM, PGD  $\ell_\infty$ , or CW on CIFAR-10, with the attack strength  $\epsilon = 8/255$  for  $\ell_\infty$  attacks and  $c = 1$  for CW.

MPN is then trained on (AT, AF, KS, WS) tuple by merging AT into the attribute classification task. We conduct experiments considering different architectures mentioned in Table 2 on CIFAR-10 and CIFAR-100, with  $\delta$  and  $\delta_{\text{PEN}}$  as MPN’s inputs, respectively. We summarize the in-distribution generalization results in Table A2, Table A3, Table A4, and Table A5. Weighted accuracy refers to the testing accuracy defined in Sec. 5, *i.e.*,  $\sum_i (N_i \text{TA}(i)) / \sum_i N_i$ , where  $N_i$  is the number of classes of the model attribute  $i$ , and  $\text{TA}(i)$  is the testing accuracy of the classifier associated with the attribute  $i$  (Fig. 3). In the above tables, we also show the testing accuracy for each attribute, *i.e.*,  $\text{TA}(i)$ . Combined accuracy refers to the testing accuracy over all victim model attribute-combined classes, *i.e.*, 135 classes for 5 AT classes, 3 AF classes, 3 KS classes, and 3 WS classes. The insights into model parsing are summarized below: (1) MPN trained on  $\delta$  and  $\delta_{\text{PEN}}$  can effectively classify all the attributes AT, AF, KS, WS in terms of per-attribute classification accuracy, weighted testing accuracy, and combined accuracy. (2) Compared to AT, AF, and KS, WS is harder to parse.

Table A2. MPN performance (%) on different attack types given different evaluation metrics with adversarial perturbation  $\delta$  as input on CIFAR-10.

| Metrics           | Attack types       |                    |                     |                     |                    |                    |                     |                     |                   |                  |                   |                  |           |         |          |
|-------------------|--------------------|--------------------|---------------------|---------------------|--------------------|--------------------|---------------------|---------------------|-------------------|------------------|-------------------|------------------|-----------|---------|----------|
|                   | FGSM               |                    |                     |                     | PGD $\ell_\infty$  |                    |                     |                     | PGD $\ell_2$      |                  |                   |                  | CW        |         |          |
|                   | $\epsilon = 4/255$ | $\epsilon = 8/255$ | $\epsilon = 12/255$ | $\epsilon = 16/255$ | $\epsilon = 4/255$ | $\epsilon = 8/255$ | $\epsilon = 12/255$ | $\epsilon = 16/255$ | $\epsilon = 0.25$ | $\epsilon = 0.5$ | $\epsilon = 0.75$ | $\epsilon = 1.0$ | $c = 0.1$ | $c = 1$ | $c = 10$ |
| AT accuracy       | 97.77              | 97.85              | 97.91               | 97.91               | 97.23              | 96.13              | 96.16               | 94.22               | 99.77             | 99.64            | 99.37             | 99.12            | 96.73     | 97.30   | 97.28    |
| AF accuracy       | 95.67              | 95.73              | 95.79               | 95.71               | 95.86              | 95.26              | 95.77               | 94.05               | 99.51             | 99.36            | 99.04             | 98.68            | 95.12     | 94.84   | 94.68    |
| KS accuracy       | 98.66              | 98.66              | 98.65               | 98.71               | 98.22              | 97.55              | 97.43               | 95.52               | 99.83             | 99.79            | 99.64             | 99.48            | 96.94     | 98.13   | 98.09    |
| WS accuracy       | 87.16              | 87.16              | 87.29               | 87.52               | 84.36              | 79.99              | 80.01               | 71.68               | 98.51             | 97.83            | 96.86             | 95.57            | 88.42     | 85.28   | 85.03    |
| Weighted accuracy | 95.24              | 95.28              | 95.34               | 95.38               | 94.39              | 92.79              | 92.89               | 89.63               | 99.46             | 99.23            | 98.82             | 98.34            | 94.65     | 94.38   | 94.27    |
| Combined accuracy | 81.85              | 82.00              | 82.19               | 82.33               | 78.65              | 73.11              | 73.33               | 62.67               | 97.79             | 96.89            | 95.38             | 93.55            | 83.00     | 79.29   | 78.88    |

Table A3. MPN performance (%) on different attack types given different evaluation metrics with estimated perturbation  $\delta_{\text{PEN}}$  as input on CIFAR-10.

| Metrics           | Attack types       |                    |                     |                     |                    |                    |                     |                     |                   |                  |                   |                  | CW      |       |        |
|-------------------|--------------------|--------------------|---------------------|---------------------|--------------------|--------------------|---------------------|---------------------|-------------------|------------------|-------------------|------------------|---------|-------|--------|
|                   | FGSM               |                    |                     |                     | PGD $\ell_\infty$  |                    |                     |                     | PGD $\ell_2$      |                  |                   |                  | c = 0.1 | c = 1 | c = 10 |
|                   | $\epsilon = 4/255$ | $\epsilon = 8/255$ | $\epsilon = 12/255$ | $\epsilon = 16/255$ | $\epsilon = 4/255$ | $\epsilon = 8/255$ | $\epsilon = 12/255$ | $\epsilon = 16/255$ | $\epsilon = 0.25$ | $\epsilon = 0.5$ | $\epsilon = 0.75$ | $\epsilon = 1.0$ |         |       |        |
| AT accuracy       | 88.98              | 95.68              | 97.20               | 97.64               | 75.81              | 84.58              | 90.27               | 88.50               | 61.09             | 81.41            | 87.80             | 90.48            | 56.10   | 64.11 | 64.30  |
| AF accuracy       | 83.48              | 92.21              | 94.56               | 95.22               | 74.95              | 85.04              | 90.72               | 89.81               | 57.62             | 76.90            | 83.95             | 87.36            | 54.61   | 58.77 | 58.98  |
| KS accuracy       | 91.57              | 96.63              | 97.96               | 98.41               | 81.10              | 88.18              | 92.67               | 90.99               | 67.85             | 84.50            | 89.93             | 92.18            | 62.46   | 69.81 | 70.15  |
| WS accuracy       | 69.99              | 81.42              | 84.92               | 86.59               | 56.07              | 63.92              | 70.19               | 64.80               | 50.09             | 67.26            | 74.02             | 77.70            | 46.40   | 47.53 | 47.77  |
| Weighted accuracy | 84.29              | 92.08              | 94.17               | 94.92               | 72.53              | 81.02              | 86.58               | 84.23               | 59.44             | 78.07            | 84.48             | 87.44            | 55.07   | 60.63 | 60.87  |
| Combined accuracy | 54.83              | 72.66              | 78.63               | 80.83               | 32.59              | 46.05              | 57.10               | 50.60               | 18.38             | 45.39            | 57.10             | 63.00            | 14.62   | 19.44 | 19.70  |

Table A4. MPN performance (%) on different attack types given different evaluation metrics with adversarial perturbation  $\delta$  as input on CIFAR-100.

| Metrics           | Attack types       |                    |                     |                     |                    |                    |                     |                     |                   |                  |                   |                  | CW      |       |        |
|-------------------|--------------------|--------------------|---------------------|---------------------|--------------------|--------------------|---------------------|---------------------|-------------------|------------------|-------------------|------------------|---------|-------|--------|
|                   | FGSM               |                    |                     |                     | PGD $\ell_\infty$  |                    |                     |                     | PGD $\ell_2$      |                  |                   |                  | c = 0.1 | c = 1 | c = 10 |
|                   | $\epsilon = 4/255$ | $\epsilon = 8/255$ | $\epsilon = 12/255$ | $\epsilon = 16/255$ | $\epsilon = 4/255$ | $\epsilon = 8/255$ | $\epsilon = 12/255$ | $\epsilon = 16/255$ | $\epsilon = 0.25$ | $\epsilon = 0.5$ | $\epsilon = 0.75$ | $\epsilon = 1.0$ |         |       |        |
| AT accuracy       | 97.70              | 97.76              | 97.76               | 97.75               | 97.03              | 95.40              | 95.23               | 92.52               | 99.59             | 99.29            | 98.91             | 98.50            | 93.84   | 96.23 | 96.30  |
| AF accuracy       | 95.17              | 95.14              | 94.96               | 95.11               | 94.79              | 93.73              | 93.87               | 91.87               | 99.14             | 98.63            | 97.97             | 97.31            | 90.83   | 92.32 | 92.47  |
| KS accuracy       | 97.66              | 97.65              | 97.69               | 97.62               | 96.75              | 95.16              | 94.44               | 91.25               | 99.62             | 99.43            | 99.16             | 98.70            | 93.11   | 95.77 | 95.81  |
| WS accuracy       | 81.13              | 80.77              | 80.90               | 80.94               | 76.57              | 69.85              | 68.16               | 59.42               | 96.58             | 95.04            | 92.70             | 90.43            | 76.61   | 74.64 | 74.77  |
| Weighted accuracy | 93.60              | 93.54              | 93.53               | 93.55               | 92.11              | 89.52              | 88.97               | 85.02               | 98.85             | 98.27            | 97.43             | 96.56            | 89.34   | 90.67 | 90.76  |
| Combined accuracy | 75.08              | 74.76              | 74.82               | 74.95               | 69.72              | 61.27              | 59.31               | 48.37               | 95.27             | 93.06            | 89.89             | 86.73            | 67.19   | 66.24 | 66.56  |

Table A5. MPN performance (%) on different attack types given different evaluation metrics with estimated perturbation  $\delta_{\text{PEN}}$  as input on CIFAR-100.

| Metrics           | Attack types       |                    |                     |                     |                    |                    |                     |                     |                   |                  |                   |                  | CW      |       |        |
|-------------------|--------------------|--------------------|---------------------|---------------------|--------------------|--------------------|---------------------|---------------------|-------------------|------------------|-------------------|------------------|---------|-------|--------|
|                   | FGSM               |                    |                     |                     | PGD $\ell_\infty$  |                    |                     |                     | PGD $\ell_2$      |                  |                   |                  | c = 0.1 | c = 1 | c = 10 |
|                   | $\epsilon = 4/255$ | $\epsilon = 8/255$ | $\epsilon = 12/255$ | $\epsilon = 16/255$ | $\epsilon = 4/255$ | $\epsilon = 8/255$ | $\epsilon = 12/255$ | $\epsilon = 16/255$ | $\epsilon = 0.25$ | $\epsilon = 0.5$ | $\epsilon = 0.75$ | $\epsilon = 1.0$ |         |       |        |
| AT accuracy       | 88.17              | 95.25              | 96.92               | 97.45               | 72.40              | 82.48              | 88.11               | 85.47               | 62.77             | 80.01            | 85.88             | 88.33            | 47.31   | 51.80 | 52.48  |
| AF accuracy       | 81.81              | 91.14              | 93.53               | 94.52               | 71.43              | 81.93              | 87.76               | 86.71               | 58.16             | 74.06            | 80.88             | 84.18            | 49.98   | 49.49 | 49.96  |
| KS accuracy       | 88.62              | 94.92              | 96.58               | 97.12               | 76.97              | 84.74              | 88.78               | 86.46               | 69.38             | 84.09            | 88.68             | 90.56            | 56.07   | 59.68 | 59.72  |
| WS accuracy       | 64.19              | 74.98              | 78.60               | 79.85               | 50.64              | 56.88              | 60.32               | 54.94               | 46.50             | 61.73            | 67.79             | 70.59            | 39.46   | 39.85 | 40.37  |
| Weighted accuracy | 81.76              | 89.95              | 92.19               | 92.98               | 68.51              | 77.36              | 82.22               | 79.40               | 59.71             | 75.69            | 81.53             | 84.12            | 48.08   | 50.43 | 50.90  |
| Combined accuracy | 47.75              | 65.27              | 71.05               | 73.27               | 25.56              | 37.49              | 45.28               | 38.97               | 16.27             | 38.87            | 49.04             | 54.06            | 7.31    | 9.20  | 9.59   |

## D. Correlation between transfer attack and model parsing

Although model parsing for transfer attacks presents difficulties compared to non-transfer scenarios, our model parsing method does not fail. Fig. 7(b) highlights the dominance of correct model parsing (diagonal entries) over misclassifications (off-diagonal entries). Further, to understand why attack transferability plays a role in model parsing, we extract two representative cases from Fig. 7: (1) ‘hard-to-parse’ (‘easy-to-transfer’): transfer attacks from (ReLU,3,0%) to (ReLU,3,37.5%); (2) ‘easy-to-parse’ (‘hard-to-transfer’): transfer attacks from (ReLU,3,0%) to (tanh,3,0%). Hard-to-parse attacks show stronger input gradient correlation (see Fig. A3) between the source victim model and the transfer attack target model, indicating higher transferability. Given the model attribute information is carried within the input gradient, model parsing for transfer attacks is harder.

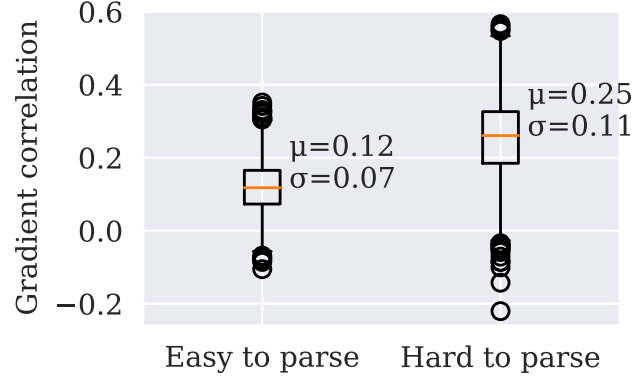


Figure A3. Input gradient correlation between true victim model and transfer attack target model in ‘easy-to-parse’ and ‘hard-to-parse’ scenarios, expanded from Fig. 7.

## E. Model parsing vs. model robustness

We re-use the collected ResNet9-type victim models in Fig. 7, and obtain their adversarially robust versions by conducting adversarial training [1] on CIFAR-10. Fig. A4 presents the generalization matrix of MPN when trained on a row-wise attack type but evaluated on a column-wise attack type. Yet, different from Fig. 6, the considered attack type is expanded by incorporating ‘attack against robust model’, besides ‘attack against standard model’. It is worth noting that every attack type corresponds to attack data generated from victim models (VMs) instantiated by the combinations of model attributes KS, AF, and WS. Thus, the diagonal entries and the off-diagonal entries of the generalization matrix in Fig. A4 reflect the in-distribution parsing accuracy within an attack type and the OOD generalization across attack types. Here are two key observations. First, the in-distribution generalization of MPN from attacks against robust VMs is much poorer (see the marked region ①), compared to that from attacks against standard VMs. Second, the off-diagonal performance shows that MPN trained on attacks against standard VMs is harder to parse model attributes from attacks against robust VMs, and vice versa (see the marked region ②). Based on the above results, we posit that model parsing is easier for attacks generated from VMs with higher accuracy and lower robustness.

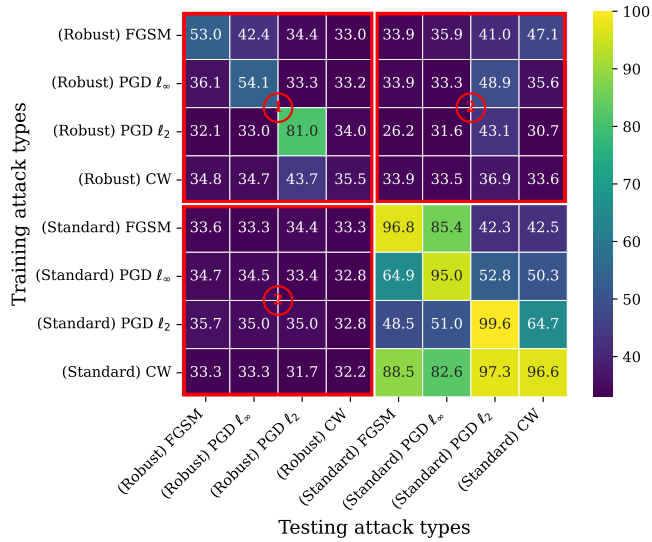


Figure A4. Generalization performance (%) matrix of MPN across attack types, ranging from FGSM, PGD  $\ell_\infty$ , PGD  $\ell_2$ , and CW attacks against standard victim models to their variants against robust victim models, termed (Standard or Robust) Attack. Other setups are consistent with Fig. 6.

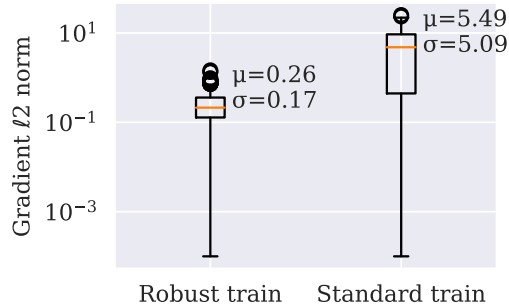


Figure A5. Distribution of input gradient  $\ell_2$  norms on testing data of robustly and normally trained models on (CIFAR10, ResNet9), expanded from Fig. A4.

To explain why the adversarial examples against robust models are hard to parse, we try to understand this from the perspective of the norm of input gradients. Fig. A5 shows that robust models are harder to infer from the adversarial examples due to the low magnitude power of input gradients, making it non-differentiable between different model attribute configurations.

## F. Other experimental studies

We also study other factors that could possibly affect the model parsing performance like PGD steps, step sizes, and stronger transfer attack methods.

Table A6. Model parsing accuracy of PGD  $\ell_\infty$  perturbations with  $\epsilon = 8/255$  on (CIFAR10, ResNet9) under different attack steps  $k$  and step sizes  $\alpha$ .

| Training \ Testing |                  |         |       |         |
|--------------------|------------------|---------|-------|---------|
|                    | $k = 10$         | 20      | 40    | 80      |
| $k = 10$           | 95.07            | 93.59   | 93.53 | 93.53   |
| 20                 | 93.73            | 93.88   | 93.92 | 93.89   |
| 40                 | 93.84            | 93.96   | 94.07 | 93.99   |
| 80                 | 93.92            | 93.98   | 94.08 | 94.11   |
| Training \ Testing |                  |         |       |         |
|                    | $\alpha = 1/255$ | 1.5/255 | 2/255 | 2.5/255 |
| $\alpha = 1/255$   | 95.07            | 91.31   | 89.33 | 88.95   |
| 1.5/255            | 93.41            | 95.85   | 95.54 | 95.18   |
| 2/255              | 91.51            | 95.88   | 96.09 | 96.02   |
| 2.5/255            | 90.26            | 95.61   | 96.09 | 96.17   |

For attacks like PGD, while hyperparameters (step count  $k$  and step size  $\alpha$ ) exist, their influence on model parsing is less notable compared to the attack strength  $\epsilon$  (Fig. 5). **Table A6** shows additional justification of model parsing vs.  $k$  and  $\alpha$ .

Table A7. Model parsing accuracy of MI/DMI-FGSM attacks vs. PGD  $\ell_\infty$ -attack on (CIFAR10, ResNet9), expanded from Table 4.

| Strength<br>( $\epsilon$ ) | Attack<br>methods | Accuracy (%)  |                       |          |
|----------------------------|-------------------|---------------|-----------------------|----------|
|                            |                   | $\mathbf{x}'$ | $\delta_{\text{PEN}}$ | $\delta$ |
| 8/255                      | PGD               | 66.62         | 83.20                 | 95.07    |
|                            | MI                | 65.16         | 82.46                 | 94.33    |
|                            | DMI               | 62.65         | 81.90                 | 90.93    |
| 12/255                     | PGD               | 76.65         | 89.73                 | 94.91    |
|                            | MI                | 72.83         | 87.02                 | 93.86    |
|                            | DMI               | 71.99         | 85.05                 | 90.67    |

**Tab. A7** consistently shows that the improved transfer attacks like MI-FGSM [86] and DMI-FGSM [18] are a bit harder in model parsing than the ordinary PGD attacks. However, the model parsing ability is still prominent, proving the feasibility of our method.